The impact of the induced velocity in the near flow field of a horizontal axis wind turbine

Schmidt Paulsen, Uwe

Publication date:
1990

Document Version
Publisher's PDF, also known as Version of record

RISØ

Risø-M-2835

The Impact of the Induced Velocity in the Near Flow Field of a Horizontal Axis Wind Turbine

Uwe Schmidt Paulsen

Risø National Laboratory, DK-4000 Roskilde, Denmark
December 1989

RISØ-M-2835

THE IMPACT OF THE INDUCED VELOCITY IN THE NEAR FLOW FIELD OF A HORIZONTAL AXIS WIND TURBINE

Uwe Schmidt Paulsen
The Test Station for Wind Turbines
Department of Meteorology and Wind Energy

Abstract. The report describes extensive power performance investigation on a Vestas V20 100 kW Prototype wind turbine. The measurements carried out and reported here comprises the experimental and theoretical results on power performance and induced wind speed effects derived at different cup anemometer locations. The report reviews in a separate annex recent development of measurements and theoretical models of the flow.

December 1989
Risø National Laboratory, DK-4000 Roskilde, Denmark

The work described was carried out for the Danish Energy Agency.

ISBN 87-550-1595-6
ISSN 0418-6435

Grafisk Service Center, Risø 1990

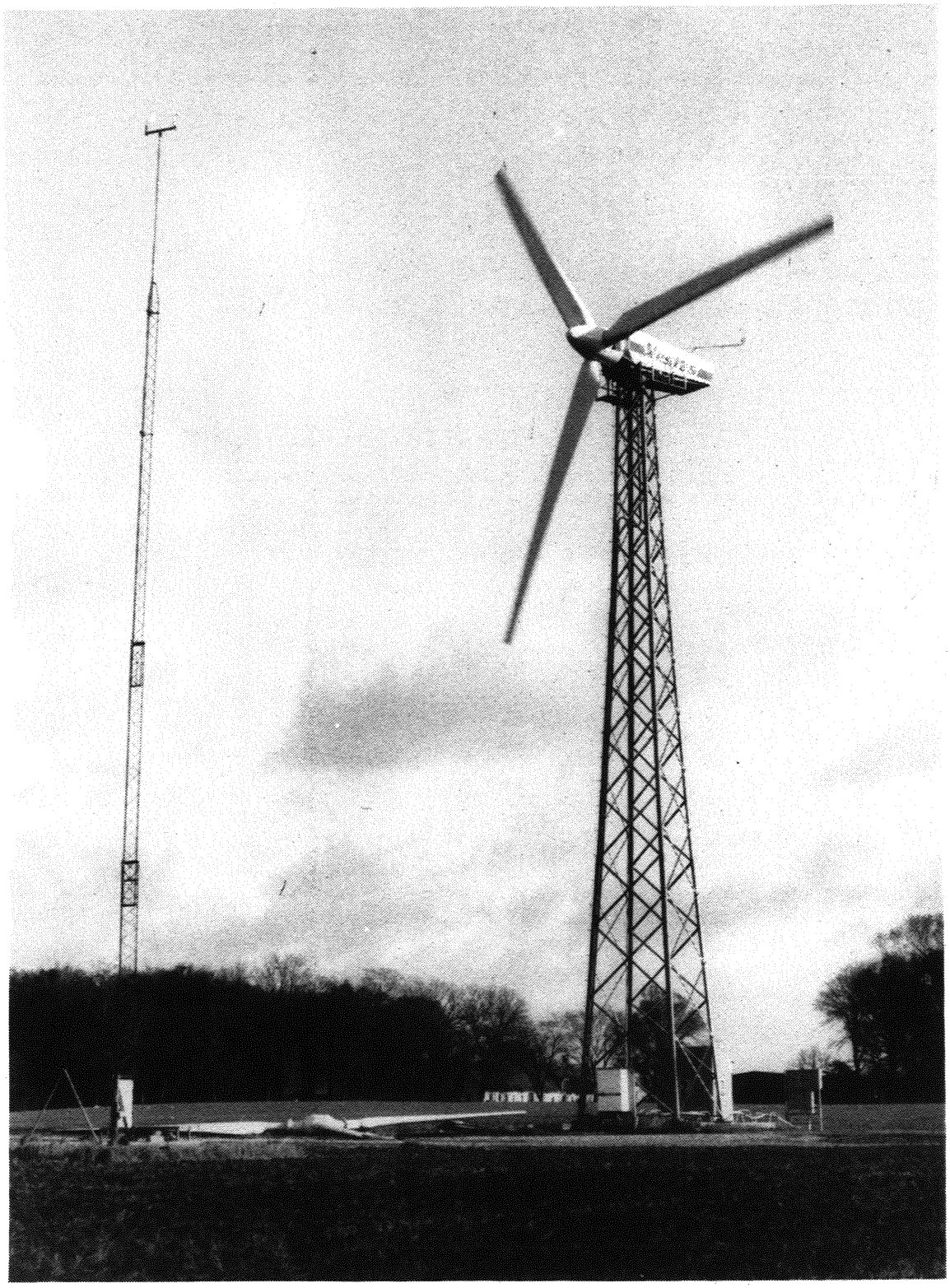

The picture shows the Vestas V20 Prototype erected at The Test Station on stand 2 with the Mobile mast to the left.

CONTENTS **Page**

NOMENCLATURE

A Scale parameter for a Weibull distribution

C Form parameter for a Weibull distribution

V Annual mean wind speed; Virtual(local) wind speed at a specified distance from the wind turbine

C_E Overall turbine efficiency; electric power interrelated to wind power

C_P Rotor efficiency, mechanical power interrelated to wind power

C_T Rotor Thrust coefficient, thrust interrelated to wind force

X Rotor tip speed ratio

P Electrical or mechanical power

<V> Average wind speed of sample record: $1/T \int_t^{t+T} V(t)dt$

σV Standard deviation of sample record: $1/T \int_t^{t+T} (V(t)-\langle V\rangle)^2 dt$; square root of variance $(\sigma V)^2$

a Slow-down or aerodynamic interference factor: $1-(V/V_\infty)$

f The probability for a wind direction in a certain sector

1. INTRODUCTION

The Vestas V20 Prototype wind turbine was erected at The Test Station in June 1987 on stand 2. The standard test was completed in July 1988. The measurements reported by Paulsen et al. [1] correspond to the standard measurement program, and for detailed information the reader is recommended to consult the reference. The turbine has been part of a research program targeting to quantify the influence of induced wind speeds made by the wind turbine. A difference of 1 % between indicated ie virtual wind speed measured at a certain distance from the wind turbine obviously add 3% uncertainty on the power performance determination. In order to examine these flow effects, extensive power curve measurements have been carried out and compared with theoretical models. Six meteorological masts(meteo masts) have been set-up, four of them arranged on a line with anemometers in hub height at relative distances of -2.5, -1.25, -0.68 and 1.5 rotor diameters. During the test period extending from July until September 1988, the secondary generator was electromechanically disintegrated from the system, so that the power was delivered by the primary generator. The commercial available wind turbine differs from the tested prototype on several topics. For detailed information on the particular differences, the reader should consult the manufacturer. A literature survey on flow effects for horizontal axis wind turbines is presented in a separate annex. The work summaries recent developments of theoretical models and experiments carried out on the subject and identifies the combined or interrelated problems when measuring power curves.

2. THE WIND TURBINE

In this chapter the wind turbine is described to the extent necessary to understand the measurements carried out. The principles of the control system are outlined as they are the basis for understanding the turbine operating at steady conditions.

2.1. Technical description.

The layout of the nacelle is shown in Fig. 2.1.1. The wind turbine has a three-bladed upwind rotor with fixed cantilevered GRP blades on a cast iron hub.

Yawing of the nacelle is carried out by an electrical motor controlled by a wind vane, mounted on top of the nacelle. Further specifications are listed in Table 2.1.2.

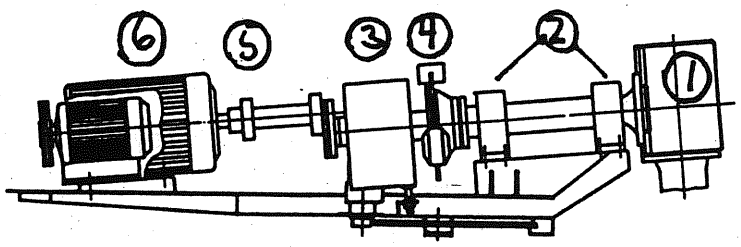

1 Hub
2 Bearings
3 Gear box
4 Disc brake
5 Clutch
6 Generator

Fig. 2.1.1. Principal lay out of the nacelle.

Table 2.1.2. Technical description of Vestas V20.

Rotor

Hub height:	24.25 m
Number of blades:	3
Rotor diameter (measured):	19.93 m
Swept area:	312 m^2
Rotor rotational speed (measured):	45.5 rpm
Tilt:	5 deg
Coning:	0 deg
Blade tip angle (measured):	- 2.1 deg
	- 2.2 deg
	- 2.1 deg

The Power control is by stall.
The Hub is made of cast iron, and no extensioners are used.
The rotor rotates clockwise when viewed from upwind location.

Blades.

Type:	Vestas V20 10 m cantilevered GRP blades
Spar material:	GRP
Shell material:	GRP
Blade length:	9.53 m
Profile blade length:	8.25 m
Root chord:	0.983 m
Tip chord:	0.4 m
Aerodynamical, effective rotor blade area:	17.11 m^2
Blade twist:	15 deg
Blade profiles:	NACA 4415 - 40
Air brakes:	The tips turn to a angle of 80 degrees by centrifugal force.

Gearbox.

Flender SZAK 1320.
Gear ratio: 45 rpm : 1000rpm

Generator.

The generator is a induction machine
for 50 Hz/380 V grid connection.
Make: Siemens 1LA6 206-6AA90Z 200L.
Nominal power 90 kW
Synchronous rotational speed: 1000 rpm

Yaw system.

Electric yaw control with a wind vane beside the nacelle controlling a yaw motor.

Mechanical brake.

Disc brake with three calipers, mounted on the rotor shaft at the gearbox. Electrohydraulic deactivation system.

Control system.

Electric control system, based on a microprocessor and a thyristor soft-cut-in system, and contractors for the generators. (see Chapter 2.2).

Manufacturer: Vestas Wind Systems A/S

Tower.

Lattice tower.	
Number of sections:	3
Tower height:	23.50 m

Weights.

Blade, incl. adaptor:	425 kg
Rotor (blades+ hub):	1725 kg
Nacelle without rotor:	4300 kg
Tower:	4250 kg
Total weight:	10275 kg

2.2. Control system and operation.

The control system is made by Vestas Wind Systems A/S. It is based on a microprocessor, which operates via a number of sensors. The high voltage part includes a thyristor/diode system on all phases.

The control system has a full automatic operation mode, where a number of parameters are supervised. For a detailed description of the parameters the operational manual should be consulted.

The automatic operation is carried out the following way. For wind speeds above 3.6 m/s the automatic yawing is activated. For increasing wind speeds and above a certain rotor rpm, automatic motor start is activated through the thyristors, and the generator is connected to the grid.

If the power for the generator is passing a lower treshold level, the generator is disconnected. The stop wind speed is at 25 m/s.

2.3. Instrumentation.

The chapter summarizes the instrumentation of the wind turbine, concerning the extensive measurements and the sensors used. The overall instrumentation is shown in Fig. 2.3.1.

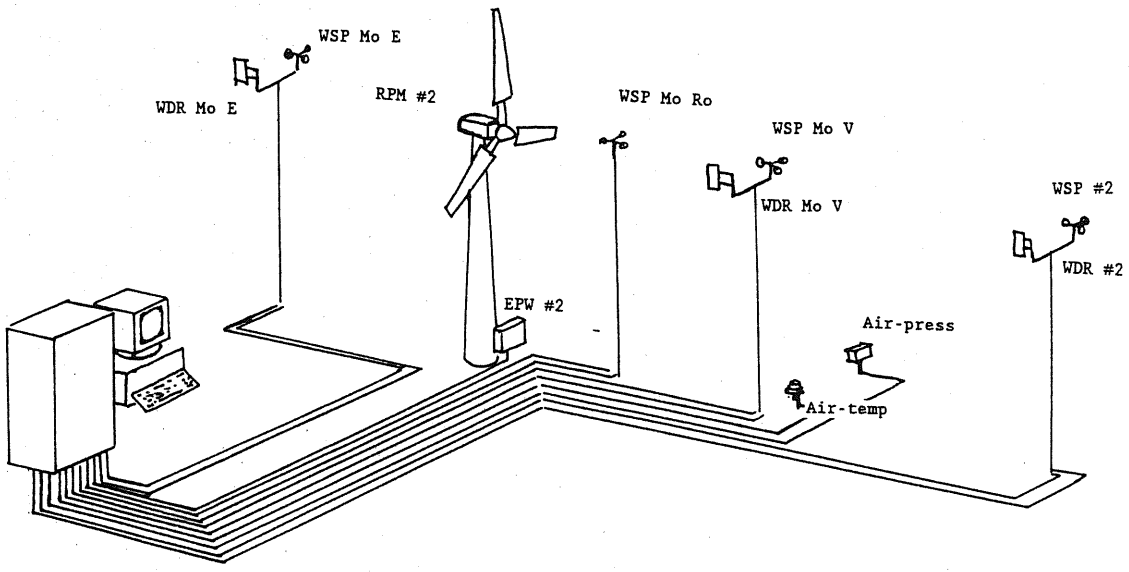

Fig. 2.3.1. Data-link system applied for the extensive measurements.

For measuring the rotational speed of the rotor a disc with 9 holes was mounted behind the primary generator with an inductive sensor to count the pulse frequency.Close to the sensor a frequency to analog converter was mounted for further data transmission.

The measurement of electric power output was carried out with three current transformers, one on each phase, and a power converter that converts the signal to a voltage signal.

Virtual wind speed was measured at six different mast locations with a cup anemometer. The rotor with three cups is giving 2 electric pulses per rotation and the pulse signal is converted into a voltage signal in another box. The anemometers have been calibrated in a wind tunnel at the Danish Maritime Institute.

The wind direction is measured with a wind vane adapted to a cos/sin resolver, and converted to a D/A signal in the voltage range from 0 volt to 3.6 volt. The output is proportional to the wind direction.

Temperature and barometric pressure are measured with two sensors with high accuracy, and they are mounted stationary at the meteorological tower and the computer room, respectively.

2.4 Power Performance and Yaw Stability.

The power curve and yaw characteristic are reviewed from reference [1] in order to present comparisons between results based on the IEA recommendations [2] on power performance procedure used at the Test Station, see chapter 3.3 and results presented in this report.

The power curve reported in the test report was measured over a period of 250 hours. The generated power was analyzed with winds from the wind sector 240 deg to 330 deg. (N). The turbulence intensity was on average 0.11-0.14. The result is shown in Fig. 2.4.1 .

POWER CURVE MEASUREMENT

WIND TURBINE: Vestas v20 100kW

Measurement setup : anemometer at hub height 2 - 4 rotor diameters from wind turbine. Allowed wind direction +- 45 deg. from anemometer mast. Data reduction by 10 min. and 30 sec. averaging times and the method of bins with a bin width of 0.5 m/s.

MEASUREMENT SUMMARY

MEASUREMENT PERIOD : 28-Aug-87 to 01-Jan-88
MEASUREMENT TIME : 250 Hours

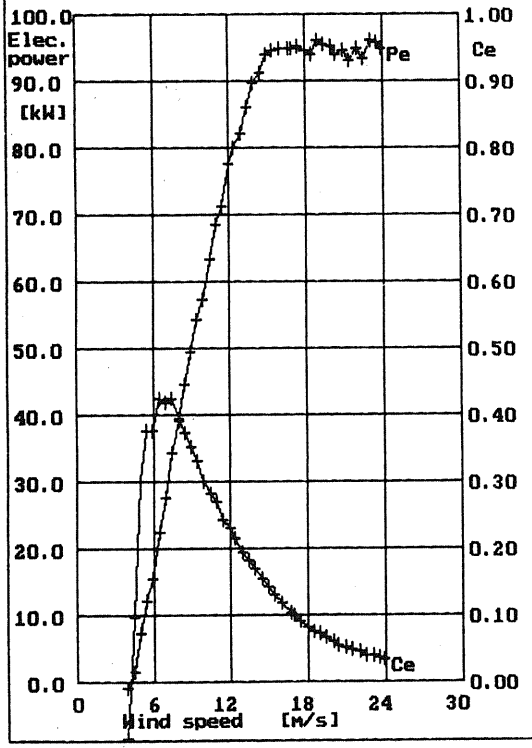

Wind speed [m/s]	Elec. power [kW]	Avg 10 min #	Ce
3.98	-1.05	28	-0.086
4.49	1.71	41	0.098
5.03	7.38	66	0.301
5.52	12.19	74	0.377
5.99	15.61	69	0.377
6.50	22.47	80	0.424
7.00	27.66	98	0.418
7.49	34.41	105	0.426
8.02	39.24	104	0.395
8.52	44.61	89	0.375
9.00	49.48	97	0.353
9.48	54.24	78	0.331
9.96	57.33	82	0.302
10.53	63.62	96	0.284
10.98	68.73	66	0.270
11.48	71.29	71	0.245
12.01	77.67	66	0.233
12.46	80.25	53	0.216
12.96	82.19	48	0.196
13.48	86.25	29	0.183
14.00	89.76	20	0.170
14.48	91.38	18	0.156
15.05	94.22	8	0.144
15.47	94.79	10	0.133
16.02	94.93	4	0.120
16.71	95.10	1	0.106
17.03	95.14	2	0.100
Wind speed	**Elec. power**	**Avg 30 sec**	**Ce**
17.43	95.28	23	0.093
18.03	94.78	18	0.084
18.52	94.20	13	0.077
18.98	96.11	20	0.073
19.51	95.60	13	0.067
20.02	95.33	14	0.062
20.46	94.03	24	0.057
20.98	94.58	14	0.053
21.45	93.06	12	0.049
22.10	94.99	6	0.046
22.54	93.48	10	0.042
23.11	96.20	2	0.041
23.55	95.97	3	0.038
23.90	95.06	5	0.036

ANNUAL ENERGY PRODUCTION

Weibull distribution (100 % availabibity) (Hub height =24.3 m)

Roughness class	Annual production [MWh]
0	308.0
1	222.2
2	174.7
3	105.1

Form factor = 1.50 Wind speed [m/s]	1.50 [MWh]	1.75 [MWh]	2.00 [MWh]	2.25 [MWh]	2.50 [MWh]
4.0	83.9	72.7	63.4	55.7	49.3
5.0	143.7	134.3	125.5	117.9	111.3
6.0	205.0	200.7	195.2	189.8	184.9
7.0	262.0	265.6	265.3	263.7	261.7
8.0	311.3	324.4	331.1	334.3	336.0
9.0	351.2	374.6	389.2	398.4	404.4
10.0	381.7	414.5	437.7	453.5	464.6
11.0	403.4	444.1	475.2	498.2	514.9

Fig. 2.4.1. Measured Power curve, overall turbine efficiency and calculated energy production. From [1].

Some additional comments are relevant before discussing power variability presented in a separate chapter.

Theoretical investigations have been made on factors influencing the power curve [3].

The power curve is defined as a relation between the power and the free stream velocity, which is supposed to be unaffected by interference from the rotor.

The ground surface at the test site is not a smooth, homogeneous area. Although the landscape raises gentle from the firth, minor hills and valleys, buildings etc. create horizontal and vertical wind gradients.

The relationship between power and wind can be derived and interpreted in several ways, as f.ex. shown in [3].

Several conditions influence the power curve determination. The relevant factors are reviewed in ref. [3]:

The main sources for uncertainty are due to machine conditions, terrain effects, data handling methods, wind speed inaccuracy and bad correlation between wind speed and power caused by wrong positioning of the anemometer.

Errors due to machine conditions, data handling methods and wind speed calibration inaccuracy are not analyzed in the present report.

Results of yaw error measurements (30-sec average)[1] are shown in Fig. 2.4.2 in order to identify yaw misalignment as a possible input, reducing the output from the wind turbine at small and medium wind speeds.

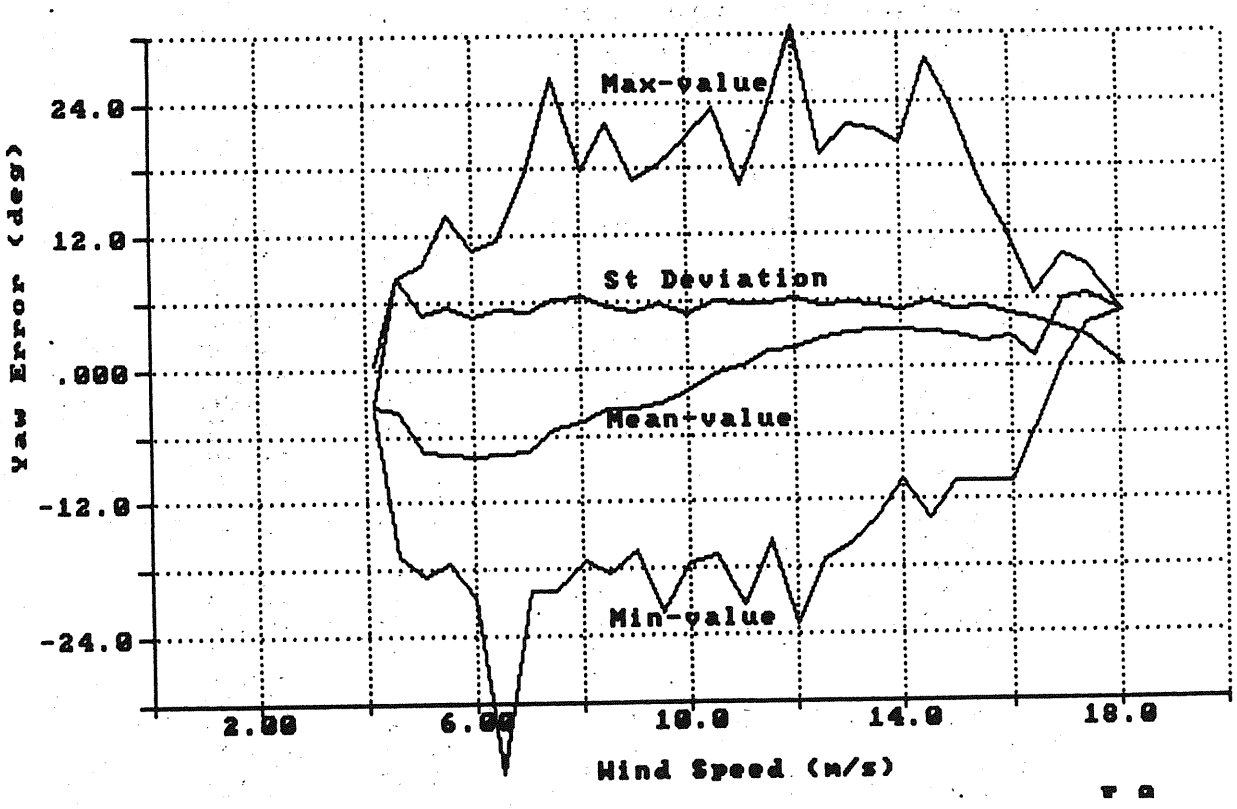

Fig. 2.4.2. Yaw error versus wind speed, derived from 30-sec averages. From [1].

The figure shows that the difference between wind direction and the yaw position is dependent on wind speed. At small wind speeds, the yaw system lags relative to wind direction by the presence of the clockwise rotating swirl induced close to the rotor plane at the position of the wind vane. At higher wind speeds, the misalignment becomes positive and indicate that the streamlines behind the rotor disc are parallel with those in front of the turbine.

From the figure the standard deviation on yaw error appears constant in the operating range considered.

2.5 Power Curve Calculations.

The wind turbine has been analyzed with an aerodynamic power performance model (ADYN_4 code, based on blade element theory (BET)). The power curve is calculated on the basis of refined N44X aerofoil data derived from [4]. The results are shown in table 2.5.1 for uniform flow over flat, homogeneous terrain.

ROTOR TILT (DEG): 0.00
ROTOR SPEED (RPM): 45.00
PITCH ANGLE (DEG): -2.10

WIND SPEED V (m/s)	SHAFT POWER P (kW)	THRUST T (KN)	T.SPEED RATIO X	SPEED RATIO 1/X	POWER COEFF. C_P	THRUST COEFF. C_T	DIM.LES COEFF. $CP*X^{-3}$	DIM.LES THRUST KT
3.0	-1.83	3.17	15.70	0.0637	-0.3530	1.830	-0.00009	0.00742
4.0	1.89	4.31	11.80	0.0849	0.1540	1.400	0.00009	0.01010
5.0	8.48	5.66	9.42	0.1060	0.3520	1.180	0.00042	0.01320
6.0	18.0	7.08	7.85	0.1270	0.4330	1.020	0.00089	0.01660
7.0	29.8	8.41	6.73	0.1490	0.4510	0.891	0.00148	0.01970
8.0	42.5	9.5	5.89	0.1700	0.4310	0.771	0.00211	0.02220
9.0	55.0	10.4	5.24	0.1910	0.3920	0.670	0.00273	0.02440
10.0	66.0	11.4	4.71	0.2120	0.3430	0.590	0.00328	0.02660
11.0	75.9	12.2	4.28	0.2330	0.2970	0.526	0.00377	0.02860
12.0	83.9	13.1	3.93	0.2550	0.2520	0.472	0.00417	0.03060
13.0	89.7	13.9	3.62	0.2760	0.2120	0.427	0.00446	0.03250
14.0	92.9	14.6	3.37	0.2970	0.1760	0.388	0.00462	0.03430
15.0	95.1	15.5	3.14	0.3180	0.1460	0.357	0.00472	0.03620
16.0	96.0	16.2	2.95	0.3400	0.1220	0.330	0.00477	0.03800
17.0	96.3	17.0	2.77	0.3610	0.1020	0.305	0.00478	0.03970
18.0	96.2	17.7	2.62	0.3820	0.0857	0.284	0.00478	0.04140
19.0	96.2	18.4	2.48	0.4030	0.0729	0.265	0.00478	0.04300
20.0	95.3	19.0	2.36	0.4240	0.0619	0.247	0.00473	0.04450
21.0	93.8	19.6	2.24	0.4460	0.0527	0.231	0.00466	0.04590
22.0	92.3	20.2	2.14	0.4670	0.0451	0.217	0.00458	0.04740
23.0	89.8	20.9	2.05	0.4880	0.0384	0.205	0.00446	0.04890
24.0	87.3	21.5	1.96	0.5090	0.0328	0.194	0.00434	0.05040
25.0	85.4	22.2	1.88	0.5310	0.0284	0.185	0.00424	0.05200
26.0	84.6	23.0	1.81	0.5520	0.0250	0.177	0.00420	0.05380
27.0	83.9	23.8	1.75	0.5730	0.0221	0.170	0.00416	0.05570
28.0	83.4	24.7	1.68	0.5940	0.0197	0.164	0.00414	0.05770
29.0	83.9	25.6	1.62	0.6150	0.0179	0.158	0.00417	0.05990
30.0	84.5	26.5	1.57	0.6370	0.0163	0.153	0.00419	0.06210
31.0	85.3	27.5	1.52	0.6580	0.0149	0.149	0.00424	0.06440
32.0	87.4	28.5	1.47	0.6790	0.0139	0.145	0.00434	0.06680

Table 2.5.1. Performance characteristics for Vestas V20, axisymmetrical flow.

Calculations have been conducted with machine conditions simulating wind direction alignment. Parametric study of yaw error influence show at optimum rotor efficiency (7 m/s) that power reductions of 3 and 12 pct are obtained at wind direction misalignment of ±8 and ±16 deg, respectively.

Power reductions obtained in uniform flow and in shear flow due to a 1/7 th power law demonstrate a difference of about 10%. In comparison, wind tunnel study with horizontal linear shear flow (see annex) show an 8% decrease of power of a propeller type model. The axial interference is then larger for uniform flow than for shear flow.

The V20 HAWT rotor is constructed with 5 deg rotor tilt and 0 deg coning. The tilt parameter contributes to power reduction to the same extent as yaw errors. As will be shown in the next chapter, terrain elevation increases the inclination of the rotor disc relative to the flow direction. Assuming ideal fluid flow approaching along the surface, a 3 deg increment would cause a power reduction of the same magnitude as the predictions above.

With a typical yaw error of 8 deg and additional increase of tilt from the terrain, calculated rotor power is reduced by a factor of $(0.97)^2 \approx 0.94$.

The local velocity should be compensated against the influence of the flow along the inclined terrain surface and calculations are provided in chapter 3.2. The windspeed error at the mobile mast 25 m in front of the turbine is calculated for the two-dimensional flow to contribute to correction with about -0.4% and +0.3% in the three-dimensional flow.

3. THE TEST STATION

The conditions for testing a wind turbine are very important for the interpretation of the results of the measurements. In the following, the conditions for the Test Station are described in chapters comprising the topography, climatology, data acquisition and analysis.

3.1. The Test Site.

The Test Station for Wind Turbines is situated at Risø National Laboratory, 5 km north of Roskilde and 30 km west of Copenhagen. The Test stands are positioned on a rather flat area close to Roskilde Fjord (see Fig. 3.1.1.). From the firth, which is about 200 m away, the ground is gently raised to an elevation of about 9 m at the stands. The prevailing winds are westerly coming from the fjord. A crossectional drawing of the elevation is provided in Fig. 3.1.2. A coordinate system with positive abscissa in downstream direction is attached to the turbine. Distances from the turbine to a meteo mast are presented as fractions of the rotordiameter.

The meteorological conditions at the site have been measured continuously on a central meteo tower over a period.

The wind speed is measured at 3, 10, 20 and 33 m height, and for the period May 1982 to January 1986 the statistical wind distribution has been calculated.

For the four heights the Weibull parameters for the wind speed distributions are shown in Table 3.1.2. Generally the measured distributions fit very well to the Weibull distributions.

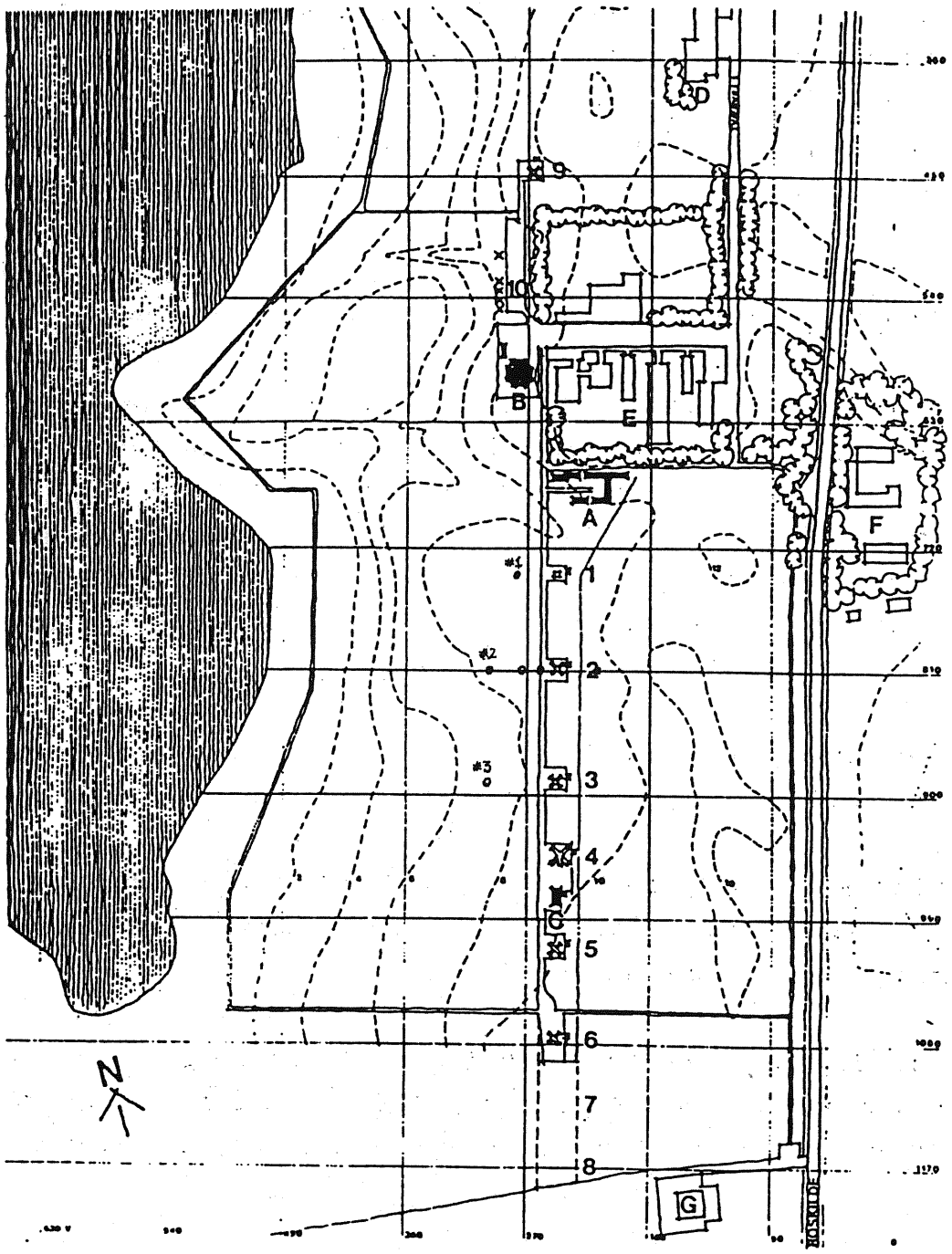

Fig. 3.1.1. Topography at the site.

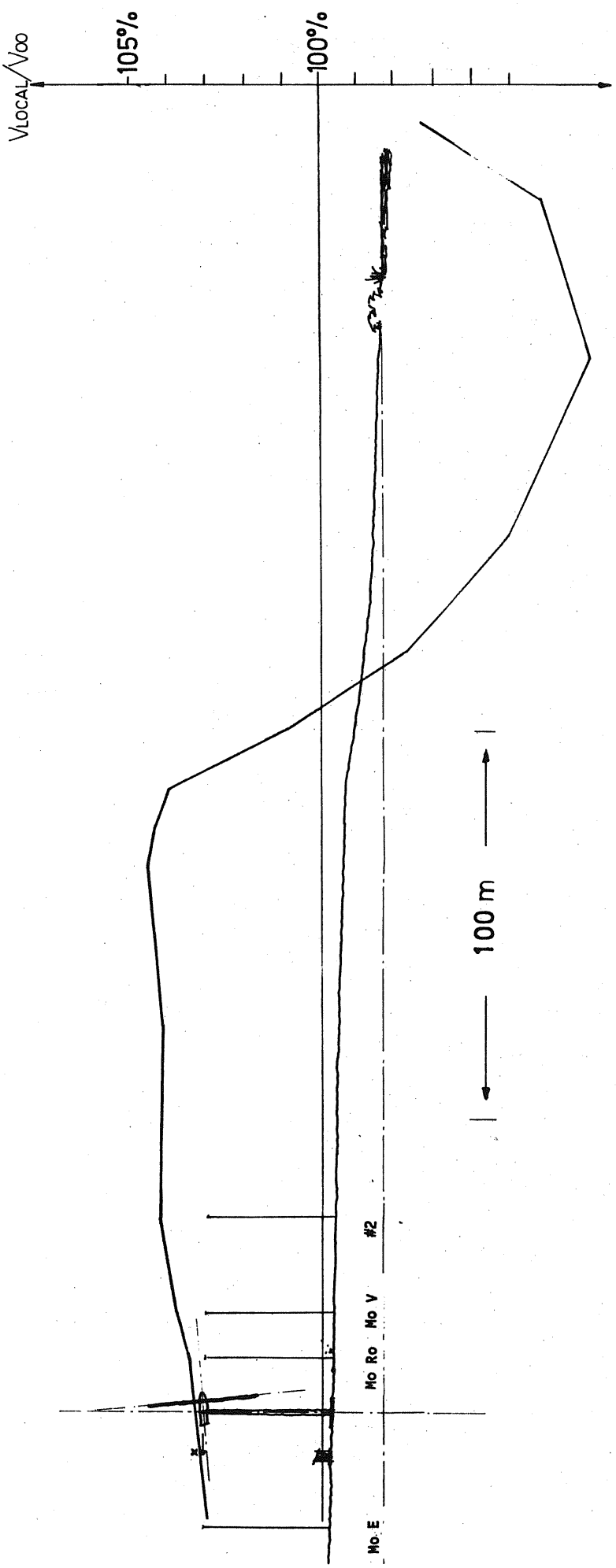

Fig. 3.1.2. Sectional view of elevations at the test site, 285°.

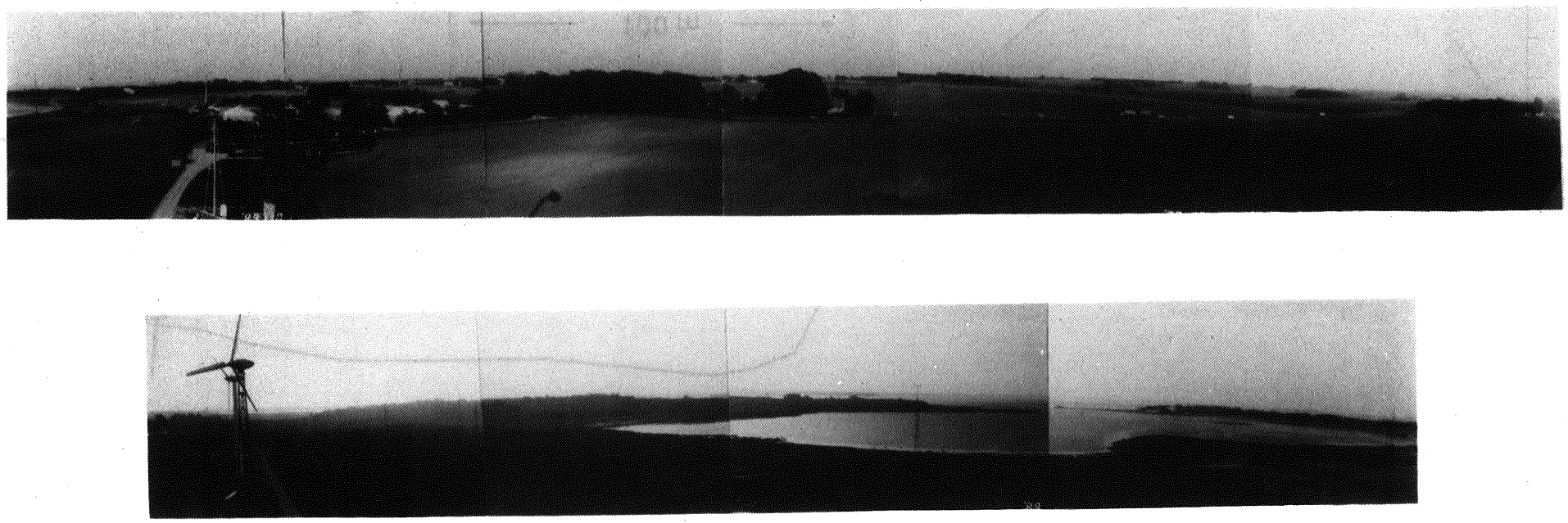

Fig. 3.1.3. Panoramic view from the hub height position.

	33 m					20 m			
	A m/s	C	f %	V m/s		A m/s	C	f %	V m/s
N	4.9	1.77	6.0	4.3	N	4.2	1.75	5.9	3.8
NE	4.1	2.04	5.0	3.6	NE	3.4	2.00	4.9	3.0
E	6.4	2.10	10.9	5.6	E	5.7	1.98	10.8	5.0
SE	7.1	2.41	17.0	6.3	SE	6.6	2.38	16.9	5.9
S	5.5	2.21	9.7	4.8	S	4.8	2.17	9.6	4.2
SV	6.2	2.34	18.2	5.5	SV	5.7	2.26	18.3	5.0
V	7.7	2.12	20.6	6.9	V	7.4	2.13	20.9	6.5
NV	6.5	1.68	12.6	5.8	NV	6.3	1.76	12.7	5.6
Total	6.5	2.00	100.0	5.7	Total	6.0	1.93	100.0	5.3

	10 m					3 m			
	A m/s	C	f %	V m/s		A m/s	C %	f m/s	V
N	3.8	1.73	5.8	3.4	N	3.2	1.71	5.6	2.9
NE	2.9	1.86	4.8	2.6	NE	2.5	1.75	4.6	2.2
E	4.8	1.87	11.9	4.3	E	3.8	1.66	13.4	3.4
SE	5.8	2.25	16.4	5.1	SE	4.7	1.97	16.6	4.1
S	4.3	2.03	9.9	3.8	S	3.5	1.88	9.9	3.1
SV	5.4	2.21	18.8	4.7	SV	4.5	2.14	17.3	4.0
V	7.1	2.17	19.8	6.3	V	5.7	2.10	20.2	5.1
NV	5.9	1.77	12.5	5.3	NV	4.8	1.80	12.3	4.2
Total	5.5	1.87	100.0	4.8	Total	4.4	1.79	100.0	4.0

Table 3.1.2. Weibull parameters for wind speed distributions at the test site.

The annual mean wind speed is 5.3 m/s at 20 m height and 5.7 m/s at 33 m. The prevailing wind directions are shown to be west and southwest, which under normal conditions are the wind directions used for the measurements on the wind turbines. Stationary masts for wind speed measurements are placed perpendicular to the row of test stands, which has an orientation from 15 deg north to 195 deg south. It is shown in Fig. 3.1.1. that mobile masts have been positioned between stationary mast and the wind turbine at testbed no 2. at distances of 13.6 m and 25 m in westerly directions. Additionally, a mobile mast is located 30 m behind the wind turbine in easterly direction.

These anemometers were arranged on top of masts at a height above ground equal to 24.5 m. The anemometer code at mast 3 was 30.5 m, whereas the anemometer on mast one was 17 m. This particular anemometer was boom arranged as the only one.

Panoramic view as seen from the hub height position has been presented in Fig. 3.1.3. The meteo mast located 2.5 rotor diameters in front of the wind turbine is arranged in the direction of 285° North. The peninsula with its 20-25 m high buildings are located about 1000-1350 in the direction of 325° North relative to the mast.

3.2 Terrain Effect Calculations.

Analysis of the approaching wind speed and the perturbations induced by the shape and roughness at the site is important for interpretation of measured wind speeds at the particular reference masts described above. A reference wind speed is strongly affected by directional influences, which are (as seen on the panoramic picture) least significant in the direction of the opening of the firth (wind direction sector 275° - 325°).

In order to quantify the wind speed corrections, a wind atlas analysis (Wasp code) of the following landscape elements have been carried out:

- Shelter influence of obstacles at the peninsula
- Influence of roughness change at the coastal line
- Pressure effects from the inclination at the site

Buildings and trees have been modelled as a porous obstacle at a distance of 1200 m relative to the meteo mast Wsp#2. The wind atlas code predicts a reduction of about 4% from the influence of the obstacle. The terrain in north direction conducts similar wind speed reductions.

In the direction of 285° the 2-D escarpment shown in Fig. 3.1.2 have been modeled by a piece-wise linear ramp with a downwind length of 1.7 km and a width of 2 km.

The variation of local wind speed relative to inshore wind is indicated in the figure. The plot demonstrates for locations above the ridge, that the wind speed decreases very little with increasing elevation in the downwind direction.

The finding agrees qualitatively with results from ideal fluid flow analysis. The local wind speed at the position of 1.25 rotor diameters in front of the rotor (-1.25D) is reduced 0.4% relative to wind speed indicated at reference mast (-2.50D).

A 3-D analysis (Wasp) carried out on the wind conditions at the site (map: 5 m elevation resolution) demonstrates that the topography in the center directions 270 and 330 deg (±15° sector) introduces speed-up effects. The wind speed at Mo V (25 m) is found to increase with 0.3 % relative to reference Wsp#2 (50 m) in the direction of 285°.

It is emphasized that the terrain contributes with a slight increase of inshore wind speed from the sectors 270° - 330°, whereas the 285° frontal approach velocity is reduced about the same degree. However, experimental evidence shows that the model tends to overestimate the wind speed effect at the ridge and that the velocity deficit downstream is not as dominant as predicted [5]. In the three-dimensional flow, meshsize representation of the surface elements will cause differences in the result. Detailed investigations of errors due to differences of geometrical input have not been carried out within this work.

3.3 Data Acquisition and Analysis.

The measurement system at The Test Station has multi-channel DC-cables from each test stand to the computer room for transferring data. The sensors are supplied with electricity from power supplies at each test stand, and the signal are transferred with a voltage range from - 5V to + 5V.

At the computer room all channels pass through a filter that protects the computer equipment from lightning. The low-pass filter module enables a cut-off frequency of 0.4 Hz or 20 Hz.

Alternatively the signals can be processed without filtering. After the filter module the signals can enter a strip chart recorder for time-trace recording, to a spectrum analyzer for frequency analyzes, or a computer for data acquisition. Before entering the computer the analog signals are converted to a 12 bit digital representation of the ±5V voltage range.

For measurements of power curves the 0.4 Hz low-pass filter and a sample frequency of 1 Hz is used. The electric power and rotor torque is corrected to a standard air density of 1.225 kg/m^3, corresponding to an air temperature of 15° C and barometric pressure of 1012.3 mbar. This is in accordance with the IEA-recommendation [2].

The sampled data are averaged with block averaging time of typically periods 30 seconds. Data analysis is then performed using the Method of Bins with a bin width of 0.5 m/s. The centers of the bins are at each half and full m/s. For each bin the wind speed, electrical power, rotor rotational speed and wind direction is averaged. Standard deviations are calculated on the electric power and wind speed. For each mast, binning is performed with the wind direction and the wind speed as the constraining parameters. Class intervals of 10 deg are used with the center of the bins at each 10 deg.

The universal choice of 30 seconds as the block averaging period is provided for analysis of the variability of the wind direction and the wind speed in terms of the wind speed reduction in front of the wind turbine. The block averaging time of 30 seconds is a compromise between continuation of data and satisfactory correlation between wind speed and power. In the annex it is shown, that factors like bias errors, yaw error of the wind turbine, block averaging time, coherence between cup anemometer and the wind turbine, the wind speed and the rotor response time affect the relationship between the wind speed measured at one particular location and the power.

The IEA recommendation for power curve measurements [2] suggests that a 90 deg sector from 240 at southwest to 330 deg at north west is included in the data analysis. Data must contain at least 200 hours of 10 minutes average data. Additionally only bins with more than 3 averages are included in the test report. The power curve presented in the test report [1] was extended by 30-sec averages at higher wind speeds, but only for at least 3 averages. It is pointed out that data from the 30-sec averages were based on far fewer operating hours, and the accuracy of these data was correspondingly lower. In the present report, the power curve is derived only from 30-sec averages of electrical power.

A correction for wind shear is not performed as the wind speed sensor is positioned at hub height at a distance of minimum two rotor diameters from the wind turbine and maximum four rotor diameters from it.

In the present analysis, no constraints on the wind direction sector are made in order to outline particular influences on the power curve from the wind variability. The wind speed is not corrected for the wind shear, speed up or slow down effects caused by terrain elevation. Block averaging time is set to 30 sec in the operating range of the wind turbine.

4. POWER PERFORMANCE MEASUREMENTS

4.1. Run Statistics.

Measurements were carried out from July to September 1988. During this period, data acquisition was conducted with winds coming from westerly and easterly directions. Tables 4.1.1 through 4.1.12 summarizes statistical figures of the runs collected.

For each run, ensemble average, standard deviation, normalized standard deviation, sample minimum and maximum are calculated with a block averaging time of 10 minutes. 24 hours of measurement corresponds to a total of 86,400 scans. Situations where sensors are not functioning are indicated by hypothetical figures.

The tables show runs with differences in channel set-up. It is also apparent from the statistics, that certain wind conditions reveal an average wind direction from the south giving a wrong impression of the true wind direction distribution during the period. In order to analyze the data with representative data in each bin, runs with identical channel set-up were appended.

In the tables following abbreviations are used:

WSP....: Wind speed
WDR....: Wind direction
#No..... Stationary meteo mast at test pad number
Mo V...: Mobile mast placed 25 m, 285° in front of the rotor
Mo Ro..: Mobile mast placed 13.6 m, 285° in front of the rotor
Mo E...: Mobile mast placed 30 m, 285° behind the rotor
EPW....: Electrical net output, not corrected for departures from standard air conditions at 15° C and 1013.3 mBar
RPM....: Rotor rotational speed
YAW....: Orientation of rotor

datafile'a:\result\outnr03.dat'

rejected scan: 0
accepted scan: 57604
total scan: 57604

ChNo	Txt	Mean	Var^.5	Var^.5/Mean	Min	Max	
1	"WSP #1 "	5.5373	1.4403	0.260108	1.4355	11.9056	[m/s]
2	"WSP #2 "	7.0984	1.5055	0.212094	2.6091	12.9458	[m/s]
3	"WSP #3 "	7.1523	1.4956	0.209112	2.5871	13.5214	[m/s]
4	"WSP Mo V "	6.7573	1.5561	0.230283	1.8311	12.6563	[m/s]
5	"WDR #1 "	283.2627	24.1520	0.085264	0.0733	359.5849	[deg]
6	"WDR #2 "	210.4899	14.0163	0.066589	176.9231	256.5324	[deg]
7	"WDR #3 "	286.6038	22.1637	0.077332	0.5617	356.1661	[deg]
8	"WDR Mo V "	285.1615	23.3824	0.081997	0.0733	358.3639	[deg]
9	"EPW #2 "	26.1536	13.5632	0.518598	-15.0183	59.9161	[kW]
10	"RPM #2 "	45.8083	0.3908	0.008532	37.1307	47.7871	[rpm]
11	"YAW #2 "	278.1482	21.6226	0.077738	237.7143	331.2527	[deg]
12	"WSP Mo Ro "	6.4700	1.5230	0.235400	1.7616	12.3750	[m/s]
13	"Air-temp "	9.4170	2.0653	0.219321	6.2088	13.4762	[Deg C]
14	"Air-press "	1004.7107	4.2494	0.004229	1002.8179	1008.5512	[m Bar]

Table 4.1.1 Statistics, run no. 3.

datafile'a:\result\outnr04.dat'

rejected scan: 0
accepted scan: 93547
total scan: 93547

ChNo	Txt	Mean	Var^.5	Var^.5/Mean	Min	Max	
1	"WSP #1 "	4.9082	1.9645	0.400257	0.7637	12.2419	[m/s]
2	"WSP #2 "	6.3597	2.2225	0.349474	1.7714	13.4432	[m/s]
3	"WSP #3 "	6.3355	2.2358	0.352903	1.6026	14.7047	[m/s]
4	"WSP Mo V "	5.9902	2.2630	0.377774	1.4544	13.3099	[m/s]
5	"WDR #1 "	269.2629	20.5448	0.076300	3.0525	359.8291	[deg]
6	"WDR #2 "	206.7948	18.4466	0.089202	166.4225	269.7192	[deg]
7	"WDR #3 "	273.1427	17.9722	0.065798	214.5299	345.6654	[deg]
8	"WDR Mo V "	271.0967	19.0454	0.070253	0.8059	357.6313	[deg]
9	"EPW #2 "	18.5828	19.1748	1.031857	-14.1810	63.9977	[kW]
10	"RPM #2 "	45.4665	2.0850	0.045858	15.3000	49.6371	[rpm]
11	"YAW #2 "	262.3910	19.5872	0.074649	210.8132	309.2747	[deg]
12	"WSP Mo Ro "	5.6870	2.2383	0.393577	1.1297	12.8676	[m/s]
13	"Air-temp "	9.5801	2.6473	0.276331	4.3333	14.2821	[Deg C]
14	"Air-press "	1010.8003	4.4354	0.004388	1003.6264	1016.7837	[m Bar]

Table 4.1.2 Statistics, run no. 4.

datafile'a:\result\outnr5.dat'

rejected scan: 5769
accepted scan: 344233
total scan: 350002

ChNo	Txt	Mean	Var^.5	Var^.5/Mean	Min	Max	
1	"WSP #1 "	3.3013	2.2178	0.671804	0.2220	15.2678	[m/s]
2	"WSP #2 "	4.7622	2.8429	0.596964	0.2790	17.4966	[m/s]
3	"WSP #3 "	4.9575	2.8583	0.576564	0.2495	17.2701	[m/s]
4	"WSP Mo V "	4.0510	2.7974	0.690542	0.2910	16.7929	[m/s]
5	"WDR #1 "	33.4097	84.2006	2.520244	0.0733	359.8291	[deg]
6	"WDR #2 "	21.0881	88.6673	4.204613	0.0733	359.8291	[deg]
7	"WDR #3 "	22.1993	86.8544	3.912483	0.0733	359.8291	[deg]
8	"WDR Mo V "	18.5535	89.4414	4.820722	0.0733	359.8291	[deg]
9	"EPW #2 "	11.9430	21.9458	1.837550	-17.9487	92.4644	[kW]
10	"RPM #2 "	31.9630	19.7966	0.619358	-0.3515	46.7140	[rpm]
11	"YAW #2 "	5.3120	74.6347	14.050296	0.0000	359.9121	[deg]
12	"WSP Mo Ro "	3.6570	2.3627	0.646077	0.2468	14.9401	[m/s]
13	"Air-temp "	10.1699	2.6048	0.256129	4.7436	16.1722	[deg C]
14	"Air-press "	1022.0473	3.1242	0.003057	1007.8897	1026.5597	[m Bar]

Table 4.1.3 Statistics, run no. 5

datafile'a:\result\outnrdat'

rejected scan: 271
accepted scan: 58182
total scan: 58453

ChNo	Txt	Mean	Var^.5	Var^.5/Mean	Min	Max	
1	"WSP #1 "	1.5747	1.0838	0.688254	0.2220	7.6749	[m/s]
2	"WSP #2 "	2.9092	1.3529	0.465059	0.3429	9.2517	[m/s]
3	"WSP #3 "	2.7843	1.5350	0.551302	0.2495	9.1006	[m/s]
4	"WSP Mo V "	1.8792	1.3113	0.697797	0.2910	8.4480	[m/s]
5	"WDR #1 "	90.2311	39.9683	0.442955	0.3175	359.8291	[deg]
6	"WDR #2 "	97.3516	40.9696	0.420841	0.0733	359.8291	[deg]
7	"WDR #3 "	99.1694	44.3652	0.447368	0.0733	359.8291	[deg]
8	"WDR Mo V "	75.1556	84.8774	1.129355	0.3175	359.8291	[deg]
9	"EPW #2 "	1.1505	6.0508	5.259171	-73.2075	42.9617	[kW]
10	"RPM #2 "	27.4353	16.0384	0.584589	-0.1665	46.3440	[rpm]
11	"YAW #2 "	103.4896	24.4251	0.236014	50.1099	154.7253	[deg]
12	"WSP Mo Ro "	1.5778	0.9284	0.588446	0.2468	6.7059	[m/s]
13	"Air-temp "	13.0755	2.9995	0.229396	9.2711	20.0110	[deg C]
14	"Air-press "	1020.5383	4.2869	0.004201	1018.2538	1021.8555	[m Bar]

Table 4.1.4 Statistics, run no. 6

datafile'a:\result\outnr07.dat'

rejected scan: 243681
accepted scan: 95412
mod 600 sec. : 159
total scan: 339093

ChNo	Txt	Mean	Var^.5	Var^.5/Mean	Min	Max	
1	"WSP #1 "	4.3151	1.9926	0.461773	0.2220	13.3346	[m/s]
2	"WSP #2 "	5.8574	2.9940	0.511147	0.7022	15.3502	[m/s]
3	"WSP #3 "	6.0843	3.0460	0.500631	0.8270	15.6798	[m/s]
4	"WSP Mo V "	3.9689	2.9015	0.731058	0.2910	14.9305	[m/s]
5	"WSP Mo E "	7.1564	1.9918	0.278332	0.7711	15.3065	[m/s]
6	"WDR #1 "	116.6258	16.2927	0.139701	12.0879	343.4676	[deg]
7	"WDR #2 "	114.3336	21.2962	0.186264	1.5873	327.5946	[deg]
8	"WDR Mo E "	114.6272	13.9940	0.122083	51.4042	159.5849	[deg]
9	"WDR Mo V "	101.5772	66.5816	0.655478	0.0733	359.8291	[deg]
10	"EPW #2 "	29.4817	18.4415	0.625521	-9.5761	76.9751	[kW]
11	"RPM #2 "	45.7560	0.9188	0.020081	29.8785	46.6400	[rmp]
12	"YAW #2 "	103.2098	15.7055	0.152171	72.3516	145.4066	[deg]
13	"WSP Mo Ro "	3.2578	2.0020	0.614541	0.3947	12.4214	[m/s]
14	"Air-temp "	17.0280	4.1083	0.241268	10.7216	24.1282	[Deg C]
15	"Air-press "	1016.4144	3.7583	0.003698	1012.3734	1020.8999	[m Bar]

Table 4.1.5 Statistics, run no. 7

datafile'a:\result\outnrdat'

rejected scan: 359
accepted scan: 349643
mod 600 sec. : 582
total scan: 350002

ChNo	Txt	Mean	Var^.5	Var^.5/Mean	Min	Max	
1	"WSP #1 "	2.7887	1.4445	0.517995	0.2220	9.9070	[m/s]
2	"WSP #2 "	4.6136	1.6847	0.365159	0.2790	11.7114	[m/s]
3	"WSP #3 "	4.5655	1.6544	0.362366	0.2495	12.2529	[m/s]
4	"WSP Mo V "	4.2436	1.7343	0.408688	0.2910	11.8504	[m/s]
5	"WSP Mo E "	3.5929	1.6179	0.450324	0.2506	11.3660	[m/s]
6	"WDR #1 "	315.1968	127.1528	0.403408	0.0733	359.5849	[deg]
7	"WDR #2 "	291.7690	118.2822	0.405397	0.1221	359.8291	[deg]
8	"WDR Mo E "	297.7628	118.4247	0.397715	0.0733	359.8291	[deg]
9	"WDR Mo V "	294.1746	120.0558	0.408110	0.0733	359.5849	[deg]
10	"EPW #2 "	6.9475	11.7044	1.684684	-75.1960	71.1144	[kW]
11	"RPM #2 "	38.0692	13.4094	0.352238	-0.5365	49.1191	[rpm]
12	"YAW #2 "	303.0651	122.5883	0.404495	0.0000	359.5604	[deg]
13	"WSP Mo Ro "	3.9848	1.7175	0.431004	0.2466	35.8139	[m/s]
14	"Air-temp "	12.8482	1.8063	0.140591	9.6667	18.2967	[Deg C]
15	"Air-press "	1005.7258	2.8810	0.002865	1002.0093	1012.7409	[m Bar]

Table 4.1.6 Statistics, run no. 8

datafile'a:\result\outnr10.dat'

rejected scan: 0
accepted scan: 30858
mod 600 sec. : 51

total scan: 30858

ChNo	Txt	Mean	Var^.5	Var^.5/Mean	Min	Max	
1	"WSP #1 "	5.6659	1.3855	0.244540	1.9685	11.1585	[m/s]
2	"WSP #2 "	9.1918	1.4790	0.160904	5.2162	13.9223	[m/s]
3	"WSP #3 "	9.1258	1.5121	0.165691	4.5189	14.2787	[m/s]
4	"WSP Mo V "	8.7682	1.5357	0.175149	4.6336	13.5696	[m/s]
5	"WSP Mo E "	5.7831	2.2066	0.381554	0.8547	12.1559	[m/s]
6	"WDR #1 "	292.3909	10.8136	0.036983	251.4042	333.9438	[deg]
7	"WDR #2 "	291.2181	9.0977	0.031240	261.9048	324.9084	[deg]
8	"WDR Mo E "	297.6375	11.3013	0.037970	36.5079	351.7705	[deg]
9	"WDR Mo V "	293.3144	9.3491	0.031874	263.6142	326.3736	[deg]
10	"EPW #2 "	45.9377	11.9635	0.260429	10.8320	69.9631	[kW]
11	"RPM #2 "	45.8737	0.2739	0.005970	45.6040	46.1590	[rmp]
12	"YAW #2 "	180.6328	11.1152	0.061535	179.8681	180.7473	[deg]
13	"WSP Mo Ro "	8.5046	1.5287	0.179749	4.1221	13.2021	[m/s]
14	"Air-temp "	18.3833	0.9995	0.054372	16.3626	19.9817	[Deg C]
15	"Air-press "	1011.0875	5.8807	0.005816	1009.2127	1013.1820	[m Bar]

Table 4.1.7 Statistics, run no. 10

datafile'a:\result\outnr11.dat'

rejected scan: 1495
accepted scan: 260419
acc. 10-min. : 434

total scan: 261914

ChNo	Txt	Mean	Var^.5	Var^.5/Mean	Min	Max	
1	"WSP #1 "	4.6288	1.4579	0.314967	0.2220	10.1125	[m/s]
2	"WSP #2 "	5.0228	1.3887	0.276488	0.8041	10.0255	[m/s]
3	"WSP #3 "	5.9490	1.6412	0.275882	0.2495	12.2340	[m/s]
4	"WSP Mo V "	4.5334	1.4089	0.310775	0.2910	10.2208	[m/s]
5	"WSP Mo E "	2.6759	1.4729	0.550433	0.2506	10.0276	[m/s]
6	"WDR #1 "	282.8132	23.2078	0.082061	0.0733	359.8291	[deg]
7	"WDR #2 "	279.1507	23.1566	0.082954	0.0733	359.8291	[deg]
8	"WDR Mo E "	303.5352	59.3865	0.195650	0.0733	359.8291	[deg]
9	"WDR Mo V "	280.8902	24.1037	0.085812	0.0733	359.8291	[deg]
10	"EPW #2 "	7.4164	10.6090	1.430484	-77.0798	54.3693	[kW]
11	"RPM #2 "	43.0130	6.9210	0.160904	-0.2775	48.4161	[rmp]
12	"YAW #2 "	76.7998	130.1376	1.694503	0.0000	358.1538	[deg]
13	"WSP Mo Ro "	4.3043	1.3804	0.320706	0.4691	12.4214	[m/s]
14	"Air-temp "	16.2262	2.6154	0.161183	11.6886	23.2637	[Deg C]
15	"Air-press "	1012.5196	1.6250	0.001605	940.8538	1019.0623	[m Bar]

Table 4.1.8 Statistics, run no. 11

datafile'a:\result\outnr12.dat'

rejected scan: 1378
accepted scan: 139388
acc. 10 min. : 232
total scan: 140766

ChNo	Txt	Mean	Var^.5	Var^.5/Mean	Min	Max	
1	"WSP #1 "	1.6103	1.1240	0.698032	0.2220	5.8350	[m/s]
2	"WSP #2 "	2.2046	1.1276	0.511464	0.2790	6.3498	[m/s]
3	"WSP #3 "	2.2263	1.1264	0.505932	0.2495	5.8820	[m/s]
4	"WSP Mo V "	1.8264	1.1216	0.614129	0.2910	6.5856	[m/s]
5	"WSP Mo E "	2.0966	1.1147	0.531661	0.2506	6.2073	[m/s]
6	"WDR #1 "	44.3309	85.3582	1.925478	0.0733	359.8291	[deg]
7	"WDR #2 "	42.8906	84.6471	1.973559	0.0733	359.8291	[deg]
8	"WDR Mo E "	39.5797	81.7551	2.065583	0.0733	359.8291	[deg]
9	"WDR Mo V "	42.2275	82.6069	1.956236	0.0733	359.8291	[deg]
10	"EPW #2 "	-0.4409	0.1089	-0.246911	-0.9942	0.0523	[kW]
11	"RPM #2 "	1.6190	6.3805	3.940895	-0.3145	40.6458	[rmp]
12	"YAW #2 "	343.3404	59.6888	0.173847	12.1264	305.8462	[deg]
13	"WSP Mo Ro "	1.9823	1.1504	0.580327	0.2466	11.1017	[m/s]
14	"Air-temp "	17.9415	2.3112	0.128817	13.4176	22.6044	[Deg C]
15	"Air-press "	1013.2579	0.2584	0.000255	1012.4469	1014.2845	[m Bar]

Table 4.1.9 Statistics, run no. 12

datafile'a:\result\outbytetp05.dat'

rejected scan: 1272
accepted scan: 232994
acc. 10-min. : 388
total scan: 234266

ChNo	Txt	Mean	Var^.5	Var^.5/Mean	Min	Max	
1	"WSP #1 "	7.8718	3.8384	0.487620	0.2220	19.7041	[m/s]
2	"WSP #2 "	8.1721	3.8000	0.465003	0.2876	19.7997	[m/s]
3	"WSP #3 "	8.3689	3.8262	0.457186	0.2495	19.9491	[m/s]
4	"WSP Mo V "	7.7565	3.8322	0.494060	0.2910	19.3716	[m/s]
5	"WSP Mo E "	6.0064	3.2437	0.540038	0.2506	19.2657	[deg]
6	"WDR #1 "	333.3333	0.0000	0.000000	333.3333	333.3333	[deg]
7	"WDR #2 "	302.6721	48.9111	0.161598	0.0733	359.8291	[deg]
8	"WDR Mo E "	305.8827	42.5949	0.139252	0.0733	359.8291	[deg]
9	"WDR Mo V "	303.4308	41.9654	0.138303	0.0733	359.8291	[kW]
10	"EPW #2 "	42.5013	28.6889	0.675012	-12.6112	86.4989	[rpm]
11	"RPM #2 "	38.9398	15.8808	0.407830	-0.0555	46.1220	[deg]
12	"WSP Mo Ro "	7.4911	3.6894	0.492501	0.2466	19.0479	[m/s]
13	"Air-temp "	13.9546	1.9851	0.142257	8.0696	17.1538	[Deg C]
14	"Air-press "	1014.5445	2.6046	0.002567	1009.9478	1018.8418	[m Bar]

Table 4.1.10 Statistics, run no. 13

datafile'a:\result\outbyte11.dat'
rejected scan: 49
accepted scan: 91009
acc. 10 min. : 151
total scan: 91058

ChNo	Txt	Mean	Var^.5	Var^.5/Mean	Min	Max	
1	"WSP #1 "	7.7583	2.0819	0.268348	2.2948	16.7341	[m/s]
2	"WSP #2 "	7.2835	2.2494	0.308830	1.5036	17.5980	[m/s]
3	"WSP #3 "	10.4320	1.8164	0.174115	5.0679	18.8132	[m/s]
4	"WSP Mo V "	5.1526	2.1848	0.424018	0.2910	16.0319	[m/s]
5	"WSP Mo E "	9.6141	2.3890	0.248488	2.5642	18.5407	[deg]
6	"WDR #1 "	333.3333	0.0000	0.000000	333.3333	333.3333	[deg]
7	"WDR #2 "	96.2604	12.7344	0.132291	1.0989	171.3065	[deg]
8	"WDR Mo E "	95.9501	9.6530	0.100605	43.8339	134.6764	[deg]
9	"WDR Mo V "	97.2152	19.9991	0.205720	6.4713	343.7118	[kW]
10	"EPW #2 "	55.5686	20.8566	0.375331	-70.6957	99.5810	[rpm]
11	"RPM #2 "	45.4650	4.2700	0.093918	-0.0925	75.7600	[deg]
12	"WSP Mo Ro "	4.6256	1.9504	0.421643	0.4412	14.1501	[m/s]
13	"Air-temp "	9.4550	0.4624	0.048900	8.6557	10.4725	[Deg C]
14	"Air-press "	1022.6675	1.0856	0.001062	1011.1238	1025.0897	[m Bar]

Table 4.1.11 Statistics, run no. 14

datafile'a:\result\outv880919.dat'
rejected scan: 0
accepted scan: 7200
accepted mean: 12
total scan: 7200

ChNo	Txt	Mean	Var^.5	Var^.5/Mean	Min	Max	
1	"WSP #1 "	12.9302	1.5537	0.120160	8.4026	18.0518	[m/s]
2	"WSP #2 "	13.0775	1.6031	0.122581	7.6201	18.5299	[m/s]
3	"WSP #3 "	13.2487	1.6107	0.121572	8.0800	19.0389	[m/s]
4	"WSP Mo V "	12.7299	1.6822	0.132147	7.3749	19.0567	[m/s]
5	"WSP Mo E "	8.3585	1.8761	0.224456	3.2343	16.1703	[deg]
6	"WDR #1 "	333.3333	0.0000	0.000000	333.3333	333.3333	[deg]
7	"WDR #2 "	281.0095	5.8377	0.020774	258.5000	300.0000	[deg]
8	"WDR Mo E "	285.3496	9.1224	0.031969	259.2000	308.5000	[deg]
9	"WDR Mo V "	283.7441	5.9017	0.020799	255.3000	302.9000	[kW]
10	"EPW #2 "	77.9581	5.8830	0.075463	47.8713	87.1283	[rpm]
11	"RPM #2 "	45.9653	0.0531	0.001155	45.7590	46.0924	[deg]
12	"WSP Mo Ro "	12.2028	1.6669	0.136600	7.3825	18.5259	[m/s]
13	"Air-temp "	14.7243	0.1233	0.008375	14.5460	15.0320	[Deg C]
14	"Air-press "	1018.5210	0.1205	0.000118	1018.0270	1018.9300	[m Bar]

Table 4.1.12 Statistics, run no. 15

4.2. Turbulence Intensity and Power Variance.

The observed wind conditions have different levels of turbulence intensity. In order to describe the interaction between the wind turbine and the virtual wind speed measured at the mast, an analysis of the turbulence intensity and power variance is provided in this chapter.

The turbulence intensity is calculated on the basis of wind data from the reference mast over a time span of 30 sec. In this sense the turbulence intensity is reduced relative to figures derived with an averaging time of 600 sec (which is the normal case).

The data from the meteo mast 2.50 rotor diameters in front of the turbine (50 m) indicate a direction sensitive turbulence intensity as shown in Fig 4.2.1. with a global minimum for winds comming from the sector 275° to 315° N.

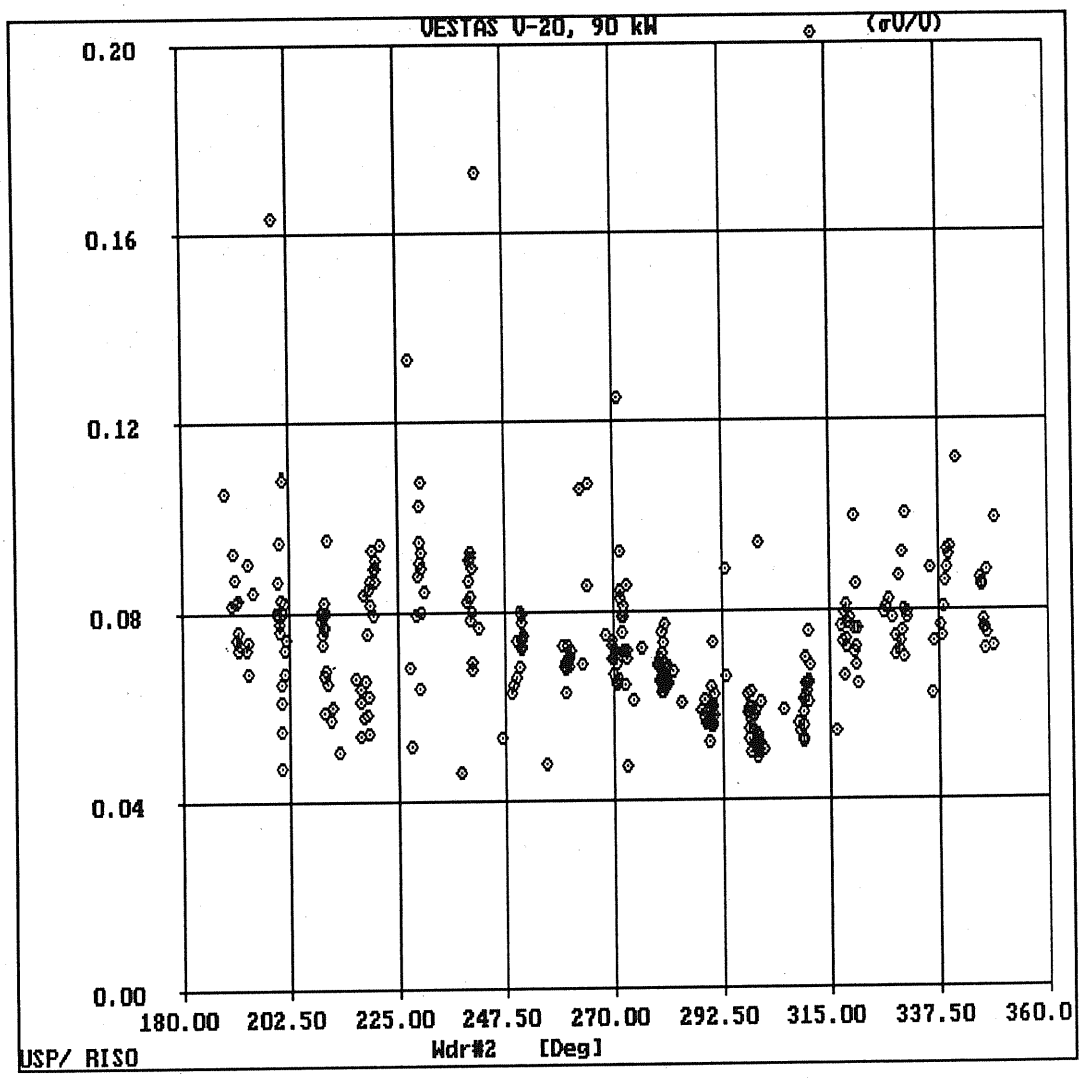

Fig. 4.2.1. Turbulence intensity in different westerly directions.

The figure shows that the turbulence intensity on the average is rather constant over the wind speed range.

For the turbulence intensity measured closer to the rotor, a 14% increase is observed from the data.

The scatter of the power at a point on the power curve is sensitive to the anemometer placement. Conventionally, scatter is related to the variance in a bin through the relation of $\sigma P/\langle P\rangle$ = constant · $\sigma V/\langle V\rangle$.

The constant term describes the slope of the power curve normalized with the power and the wind speed.

The data show that the relation above is not constant as generally assumed. The $\sigma P/\sigma V$ relation is shown in Fig. 4.2.2. In the plot σV is magnified 5 times. The slope yields the turbulence intensity.

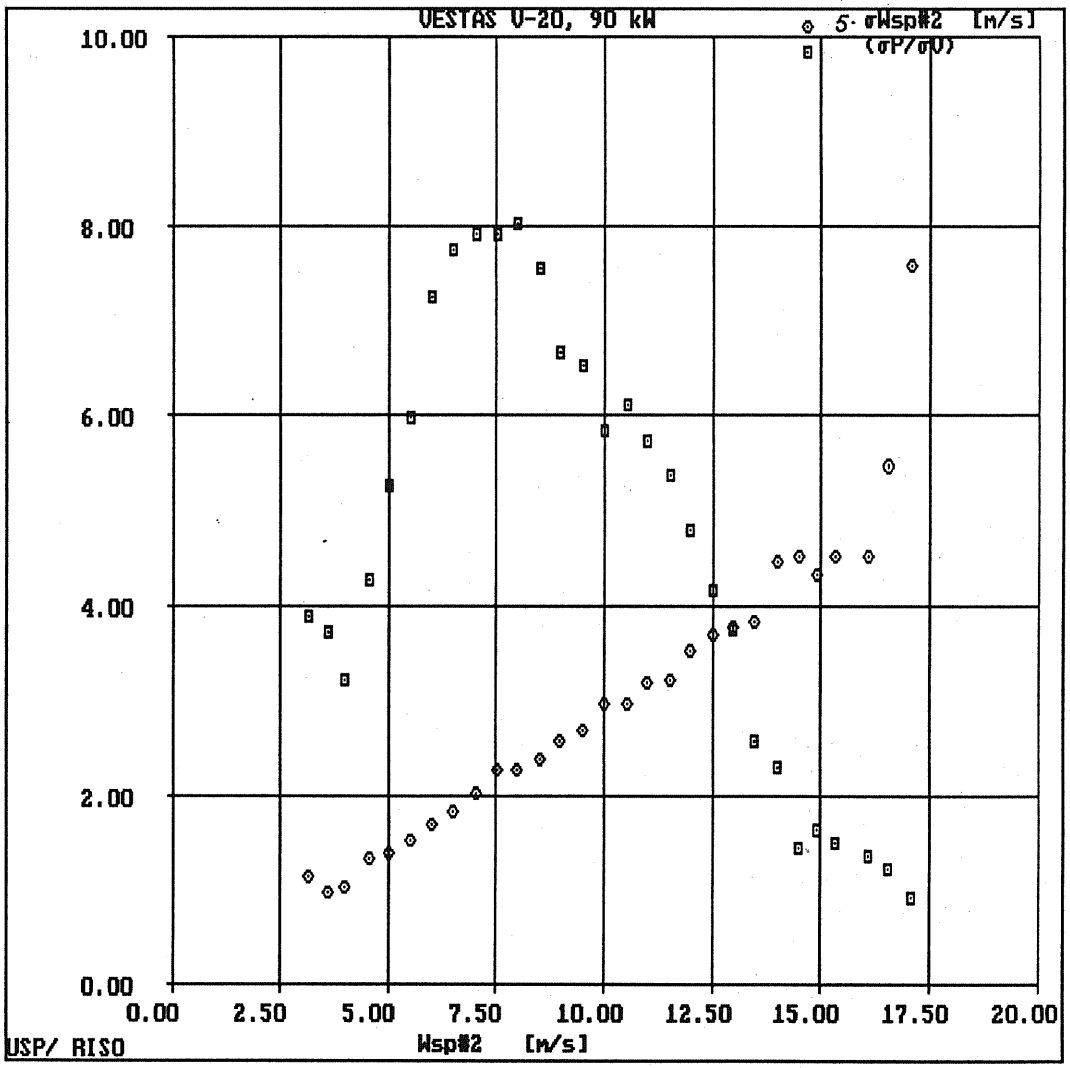

Fig. 4.2.2. $\sigma P/\sigma V$ and $5\cdot\sigma V$, mast -2.50 D. The power curve is derived in sector 285°-295°.

The plot indicates a linear relationship below optimum rotor power efficiency and a decreasing trend above optimum efficiency. At wind speeds below 4 m/s machine motoring cause an increase of σP and therefore data should be admitted in this range.

The interpretation of this finding allows is to find the scatter of the power at a given wind speed and to use the $\sigma P/\sigma V$ relationship.

Analyzing the rotor performance at the 25 m reference anemometer (-1.25D) the $\sigma P/\sigma V$ ratio shown in Fig. 4.2.2 is transformed into the relation shown in Fig. 4.2.3.

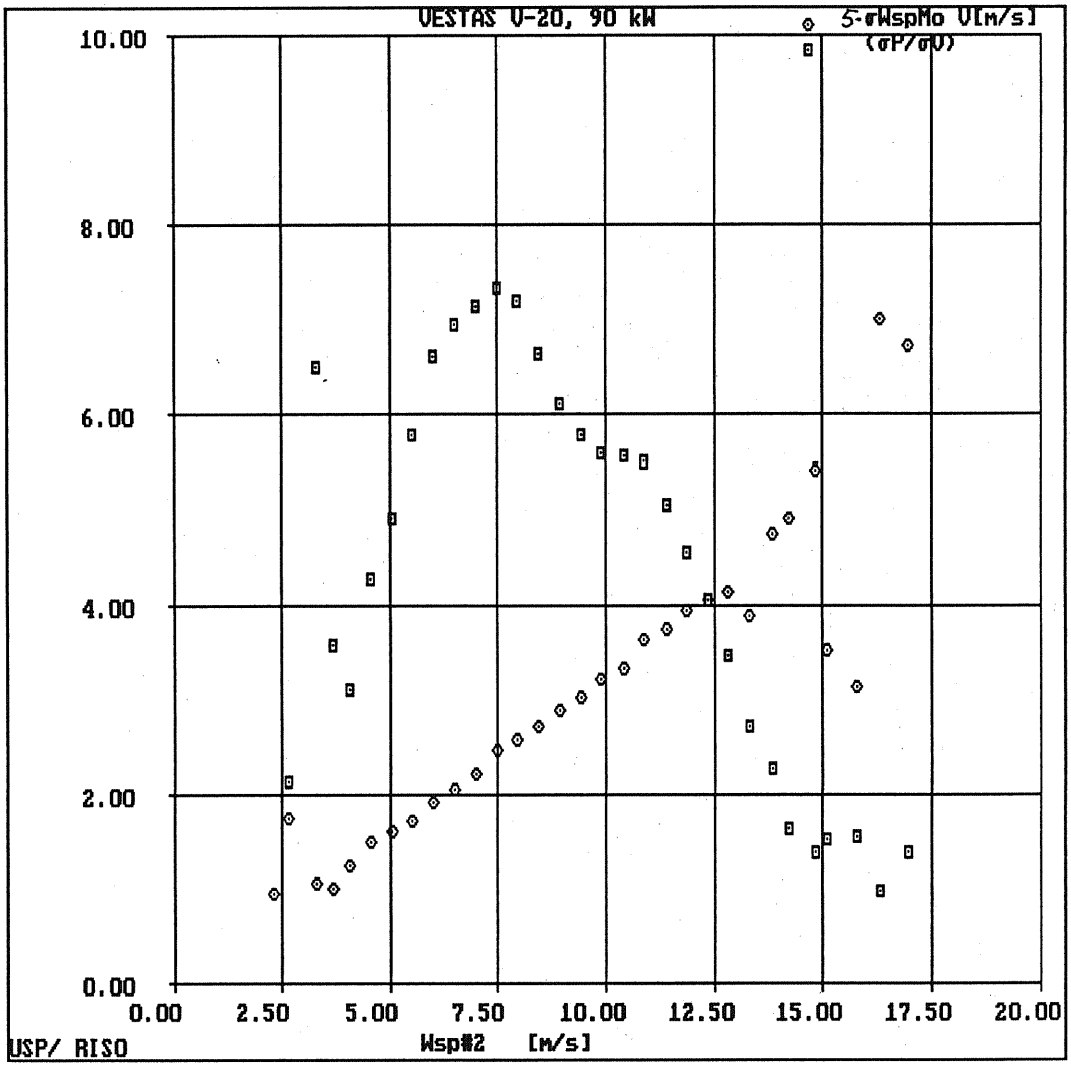

Fig 4.2.3. $\sigma P/\sigma V$ and $5 \cdot \sigma V$, mast -1.25D. The power curve is derived in sector 285°-295°.

A global maximum is decreased about 8.2% at the location -1.25D, although the turbulence intensity increases about 14 pct. The data at -0.68D reveal a decrease of $\sigma P/\sigma V$ of 6.7% relative to the figure obtained at -2.50D.

Normalizing $\sigma P/\sigma V$ with power curve gradient, a constant of 0.7074 is obtained. Performing the same procedure on data derived at -1.25D and -0.68D yields constants of 0.6522 and 0.6459, respectively. The result indicate increased (space) correlation between wind speed and power as the distance to the rotor is decreased.

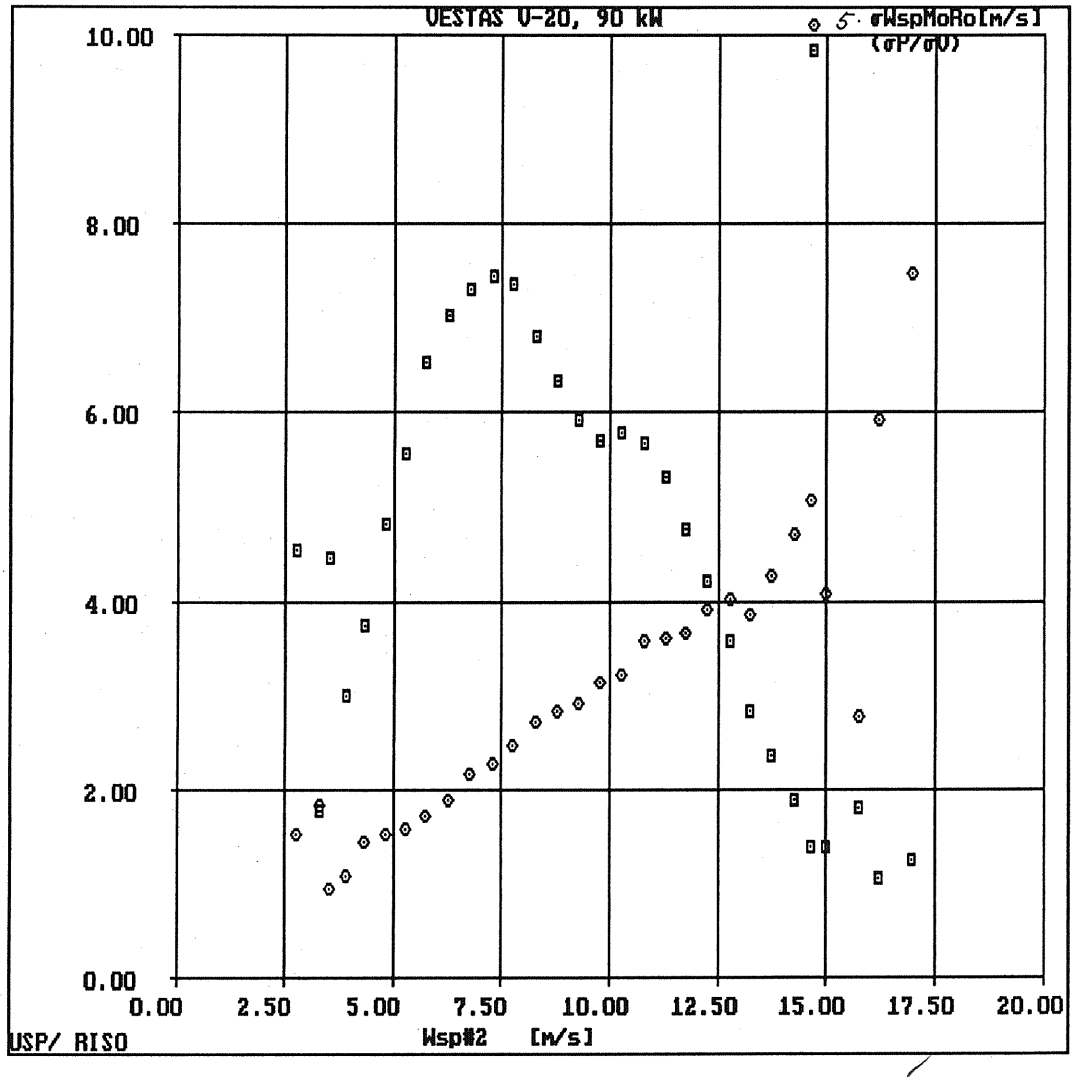

Fig. 4.2.4. $\sigma P/\sigma V$ and $5 \cdot \sigma V$, mast -0.68D. The power curve is derived for sector 285°-295°.

The fraction of $\sigma P/\sigma V$ and dP/dV is found to decrease as the distance between anemometer and rotor is reduced. The power scatter $\sigma P_{8m/s}$ derived at -2.50D is lowered from 3.1 kW to 2.2 kW at -1.25D and 1.9 kW at -0.68D, respectively.(Compare fig. 8 shown in the annex).

The results indicate that wind turbine power follows wind fluctuations. The measurements show that the power fluctuations are decreased relative to the fluctuations observed at upstream positions with a possible optimum at a distance of one rotor diameter ahead of the rotor.The decrease of power fluctuations with separation distance indicates increased (space) correlation.

4.3. Directional Power and Wind Speed Variability.

Inhomogeneous terrain characteristics like obstacles, fences, escarpments, hills etc. introduce vertical and horizontal velocity gradients, which influence the rotor. The rotor efficiency will be drastically affected by changes of the virtual wind speed and will be presented in order to demonstrate magnitudes of errors introduced.

The wind speeds measured at the test site show a directional variation following the distribution calculated on the basis of Weibull fits. Generally the wind is strong with stable periods in the direction of the firth, which is about 275-315 Deg. In the direction of north, buildings, hills and fences affect the flow. Additionally, a different type of terrain is seen by an anemometer in these different directions.

The electrical power vary with the wind direction as shown in Fig 4.3.1. Analyzing the figure, the anemometer positioned 2.5 rotor diameters ahead of the turbine measures wind speed of 7 m/s between 270° and 315° without drastic power fluctuations. In the directions of south and north terrain effects and wake interference modify the magnitude of power.

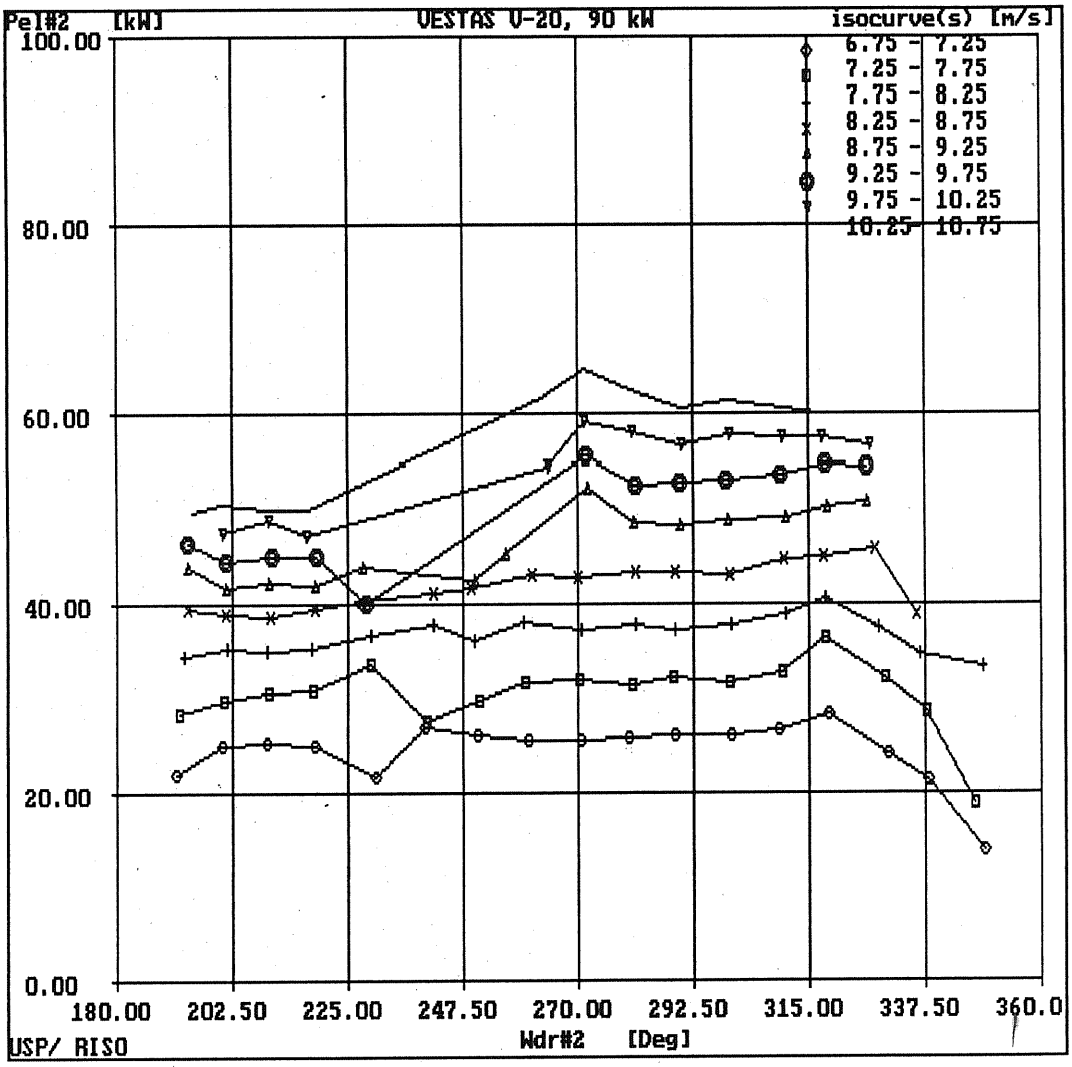

Fig.4.3.1. Directional power variability, mast at -2.50 D.

Inhomogeneity of the terrain and wind turbine operation in the wake of neighboring turbines causes a variation of the power as shown in Fig. 4.3.2. The scatter is minimized for winds blowing from the opening of the firth.

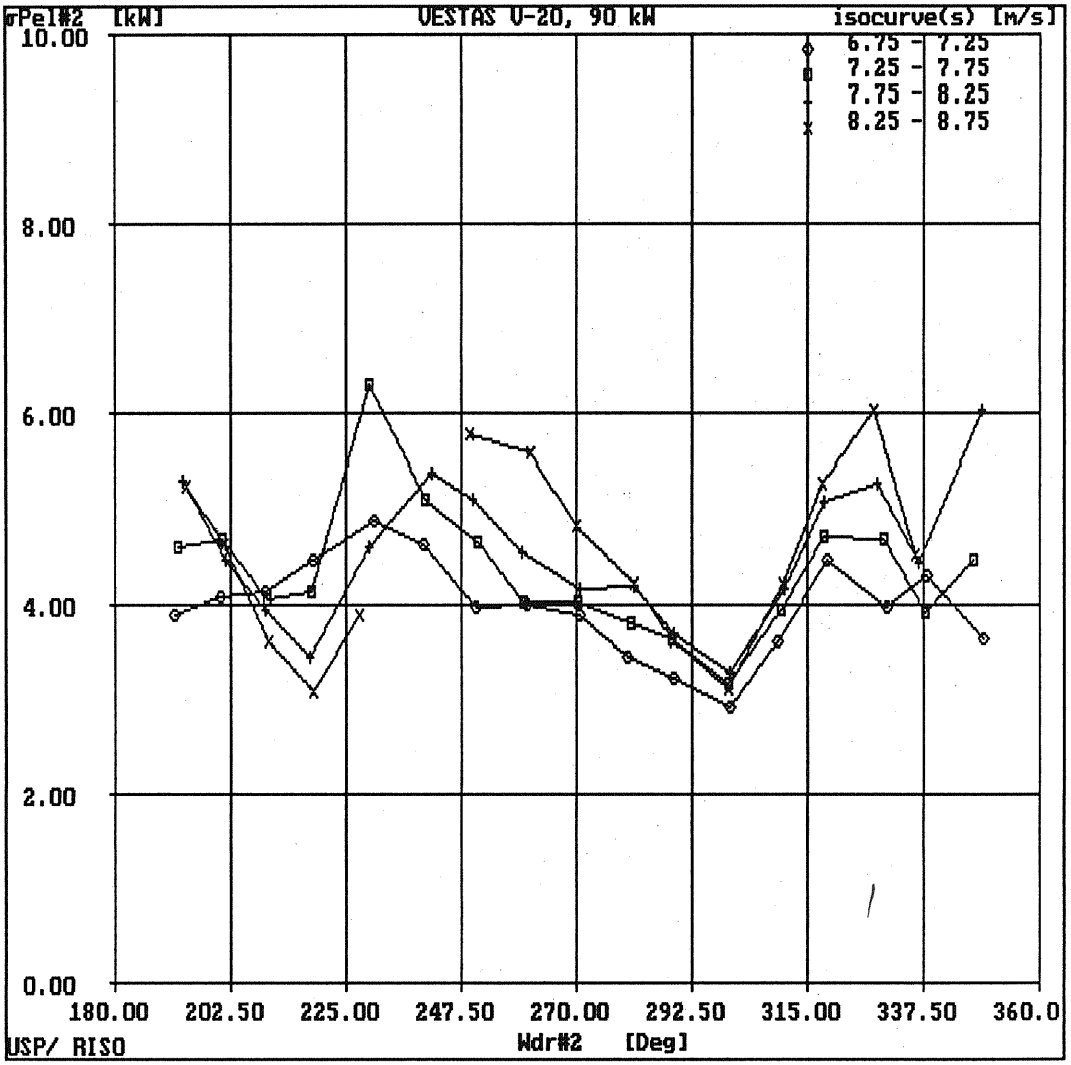

Fig. 4.3.2. The standard deviation of the electrical power, mast -2.50D.

The figures are to be compared with similar plots for the meteo mast at -1.25D.

Fig. 4.3.3. demonstrate that a higher output is measured at a given wind speed. The directional variation is changed relative to conditions at -2.50D. At 7 m/s wind speed the power difference is 4 kW in the direction of 285°.

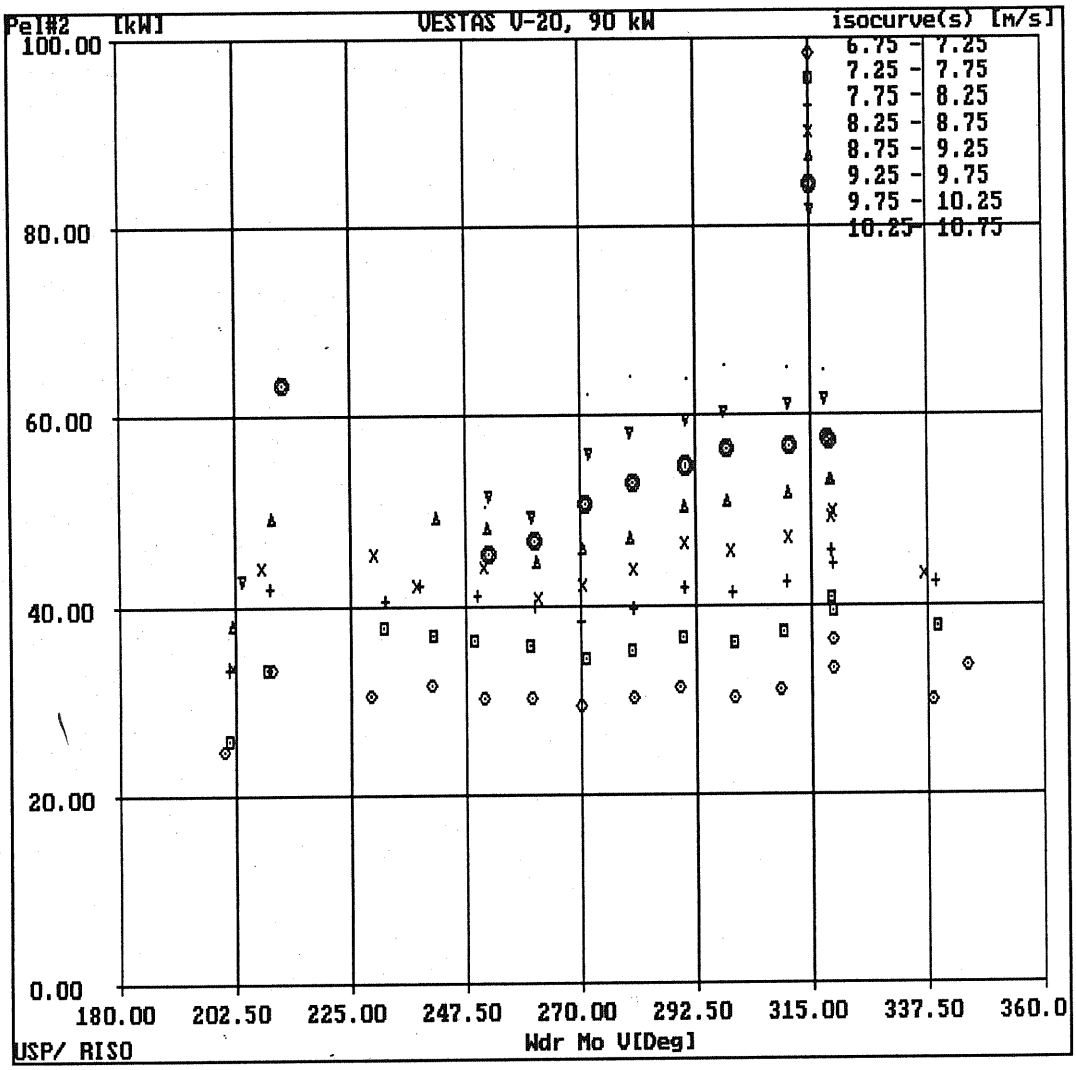

Fig. 4.3.3. Directional power quality, mast -1.25D.

The relationship between the power scatter and the wind direction is provided in Fig. 4.3.4. Although σP remains with the same magnitude, the variation of σP is less than the case was in Fig. 4.3.2.

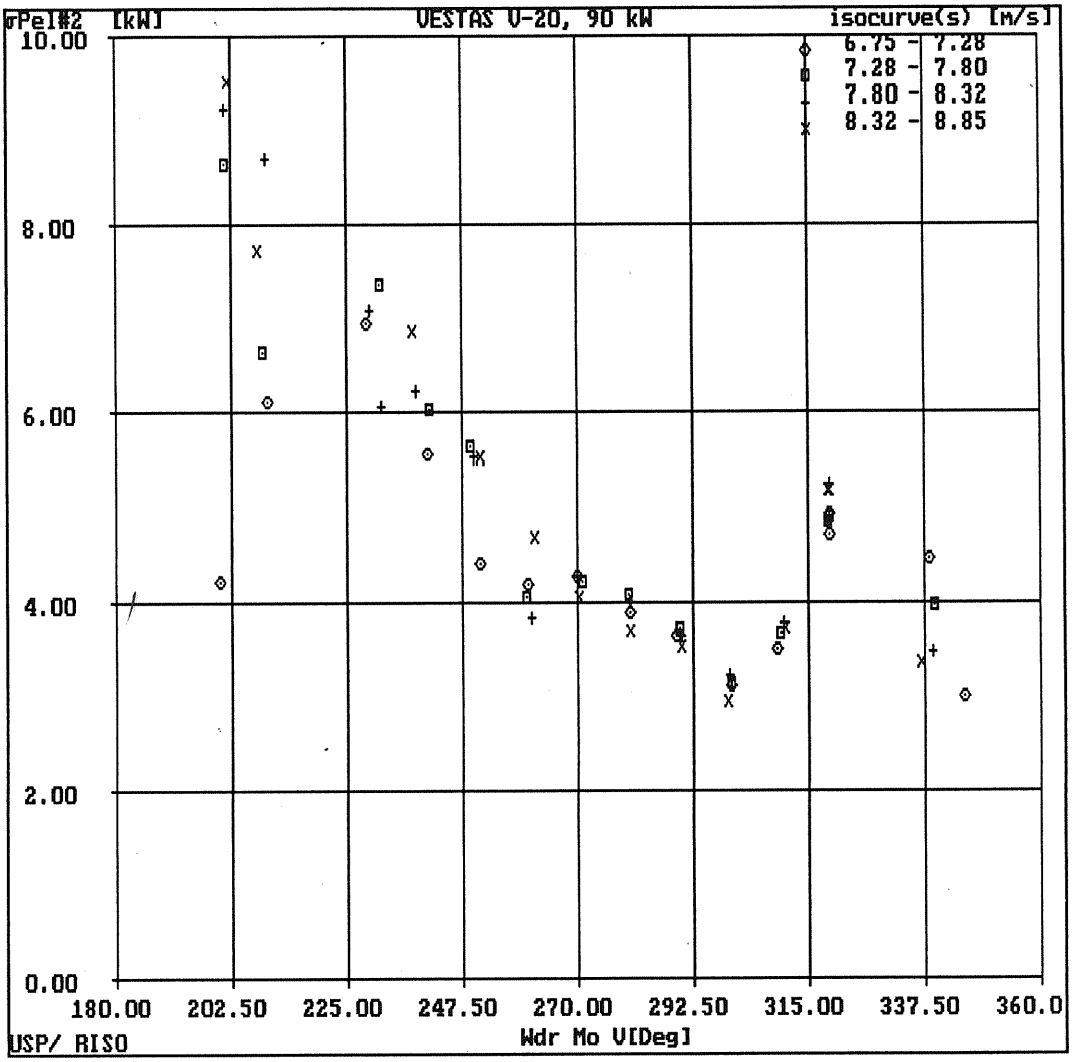

Fig. 4.3.4. Standard deviation of electrical power, mast - 1.25D.

The overall turbine efficiency C_E is by similar arguments as already presented sensitive to wind variability as shown in the following graphs. For comparison, data are evaluated at -0.68D and -2.50D in order to show variations of C_E.

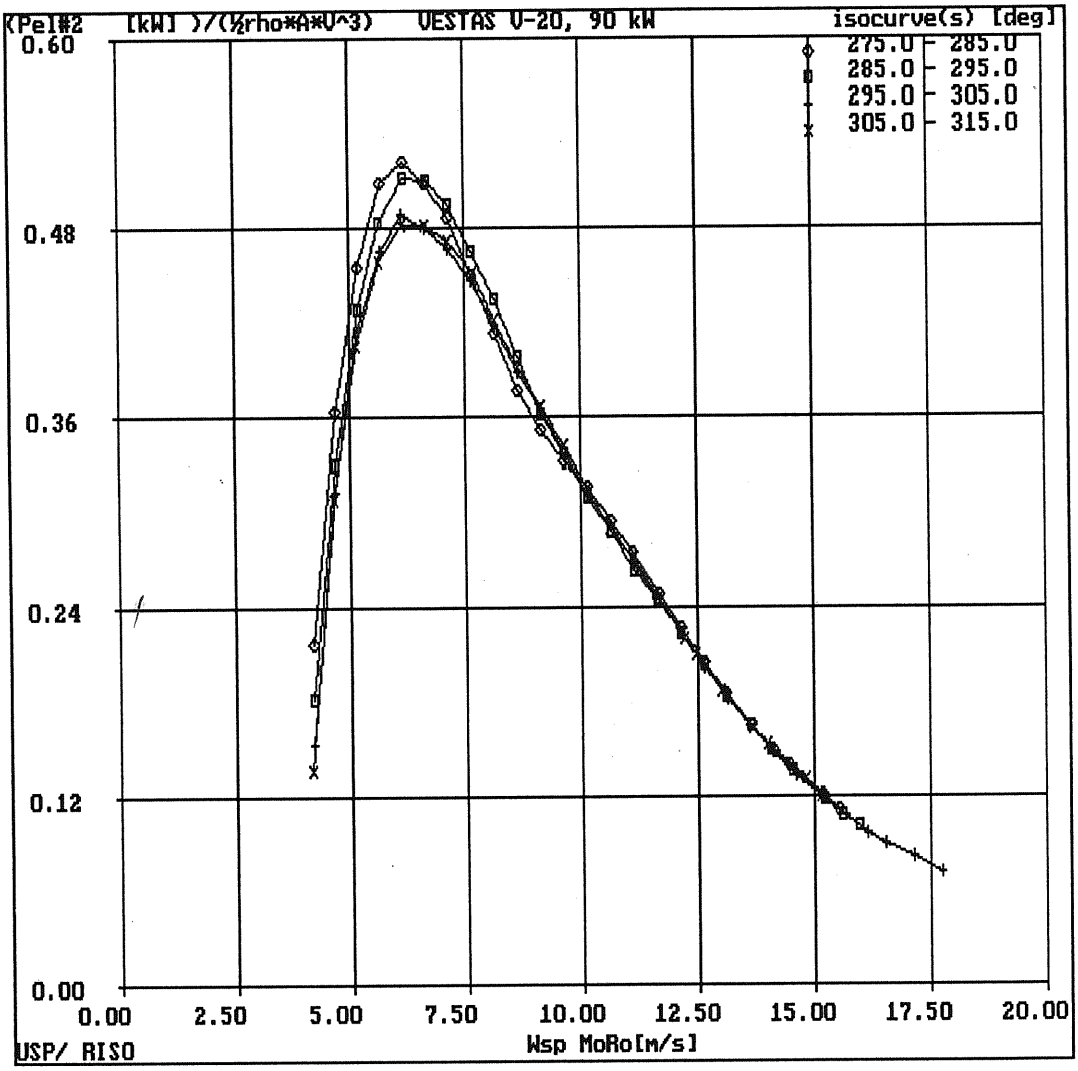

Fig. 4.3.5. Overall turbine efficiency C_E, mast -0.68D.

The winds in the direction of 285° ±10° increase C_E with 8.6% relative to a wind direction from the opening of the firth.

In Fig. 4.3.6 the same relationship is plotted for wind speeds derived at -2.50 D.

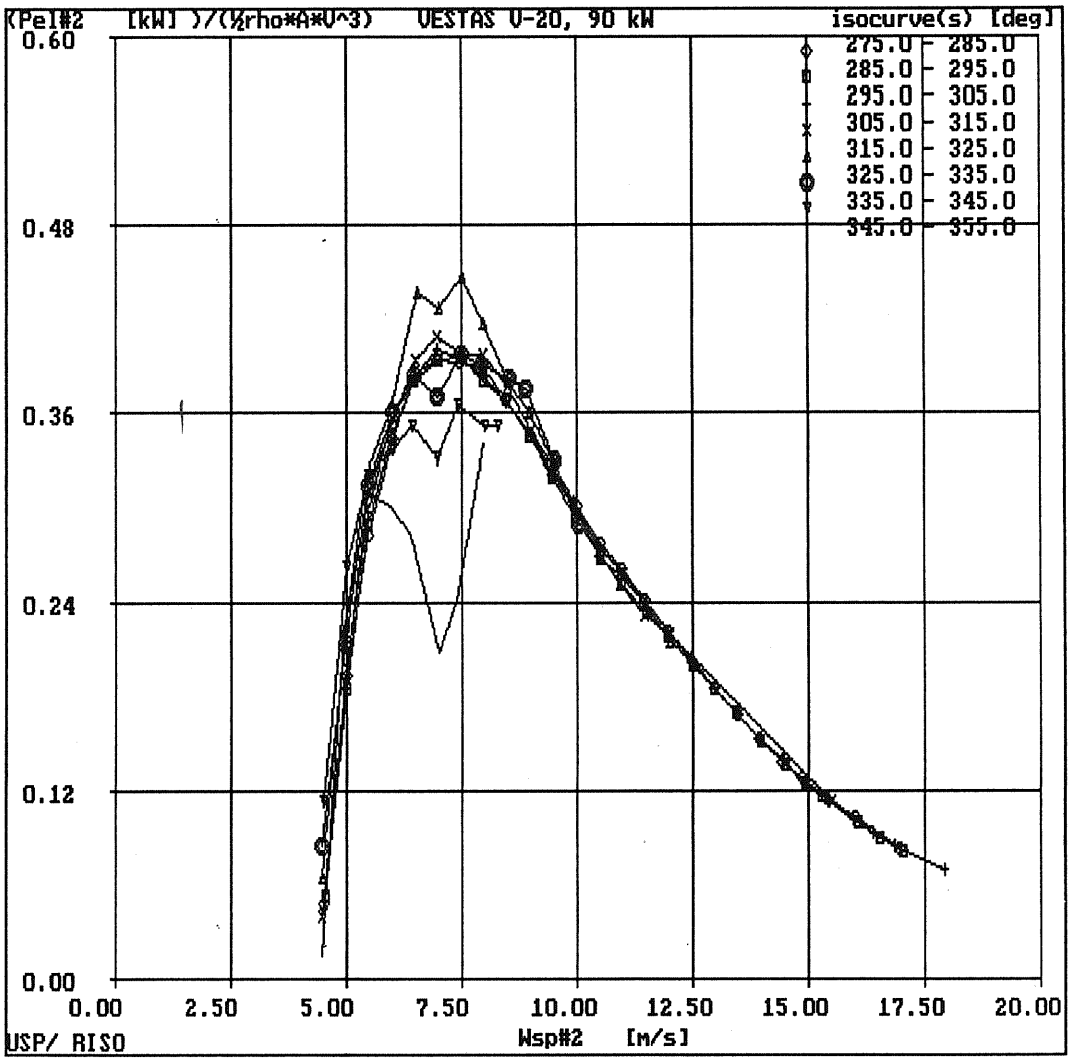

Fig. 4.3.6. Overall turbine efficiency C_E, mast -2.50 D.

The greatest difference between magnitudes of efficiency is shown to be about 0.2.

The plot demonstrates the influence of terrain effects at mean wind directions of 320°-350°.

In these directions, the orography consists of porous obstacles from buildings and trees. In northern directions, hills and buildings and another roughness length are identified.

Summarizing the results obtained, there is strong evidence to conduct power curve measurements in a wind direction with a homogenous flow.

At The Test Station, the sector 275°-315° facilitate a good interpretation of power curves since the turbulence and the terrain effects in this sector are lower than obtained for all other directions. Furthermore directions causing wake interference by neighboring turbines are to be avoided.

4.4 Flow Effects.

In the preceding chapters, site/terrain effects caused a variation of the wind speed with the wind direction. The extraction of the wind power by a rotor causes modifications on the onset flow field. At every coordinate the axial free stream velocity is superimposed with the induced velocity introduced by the presence of the wind turbine rotor.

It is evident as shown in the annex that a measured power curve with a specific anemometer position is sensitive to placement of the instrument, and that flow deficits of may be 5-10% occur.

In the present chapter results from wind speed measurements at different placements are shown in order to deduce the degree of interference. The wind speeds are inter-calibrated at conditions where the turbine did not operate. Calibration curves were succesfully conducted for wind speeds less than 7.5 m/s in the wind direction sector 275°-305°. The calibrations performed are assumed to be unaffected from wind speed conditions above 7.5 m/s and independent of meteorolocical stability in the boundary layer. The data demonstrated that differences among the cup anemometers (bearing losses) imply a recalibration in a wind tunnel.

The velocity ratio of local wind speed at -1.25D is shown in Fig. 4.4.1.

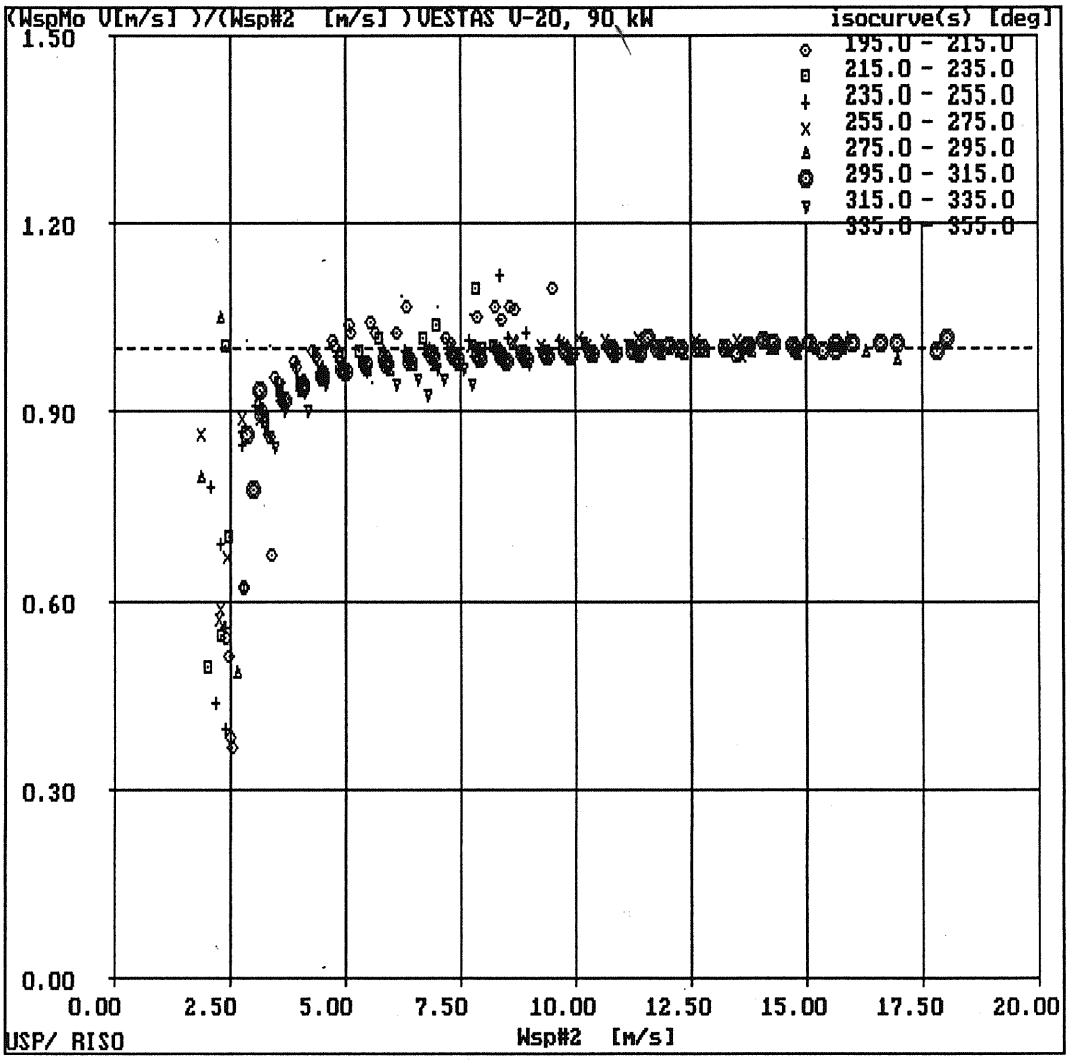

Fig. 4.4.1. Velocity ratio at anemometer position -1.25D, sector 195°-355°

In order to demonstrate the influence of the directional variability on the velocity ratio, results for sectors between 195° and 355° are shown in the figure.

At virtual wind speeds of 5 m/s, wake interference from neighboring wind turbines and terrain effects in the SW direction speeds up the local flow field, and a 5% increase of wind speed is observed at -1.25D.

Looking in NW directions, the iso-curves correlate with each other. In the case of winds emerging from 275-315 deg, results are shown in Fig. 4.4.2.

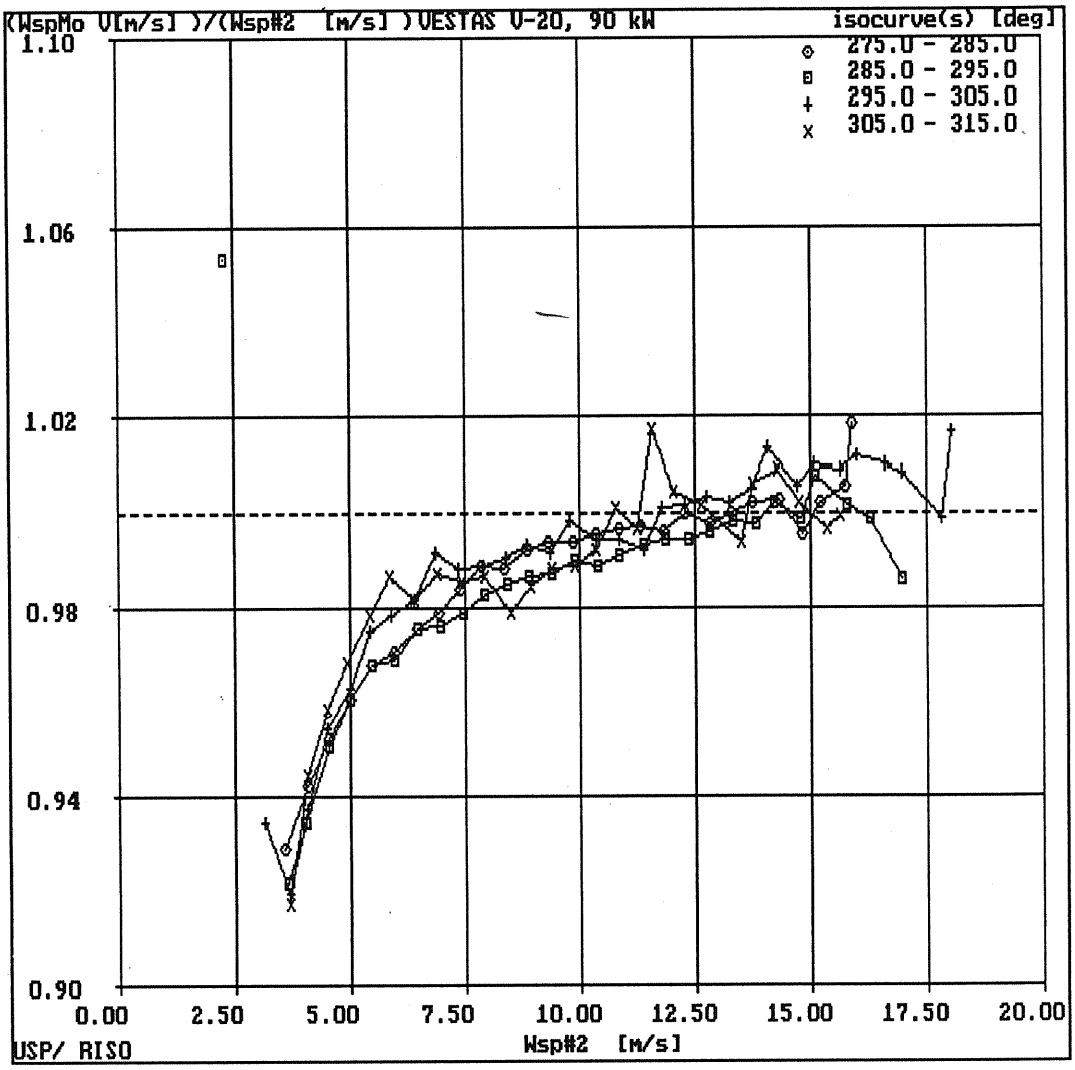

Fig. 4.4.2. Velocity ratio at anemometer position -1.25D, sector 275°-315°

The variation of the velocity ratio between these wind direction sectors is less than 1.5%. The plot demonstrate - for winds below 7.5 m/s emerging from sectors 275°-295° - that the interference factor is greater than for winds coming from the opening of the fjord.

At the optimum rotor performance, a 1.6% decrease of a virtual wind speed is measured.

Another point of view is to look at the correlation between the wind vane at -1.25D and the wind turbine direction when a wind shift occurs, which can be recalled from chapter 4.3. Since the turbine doesn't show severe misalignment errors, the apex angle of instantaneous wind directions emerging on the rotor is about 44 Deg. At the anemometer position of -2.50D the geometrical sector of incidence is about half as much. Since the average power is varying with the sector width, geometrical sectors obviously are not an adequate description of the energy capture of the wind turbine.

From these considerations it is deduced that the average interference between the rotor and the anemometer is well described for winds in the sector of 275°-315°.

The interference at the anemometer position -0.68D is described in Fig. 4.4.3. The wind direction has been obtained at the mast placed -1.25D in front of the turbine.

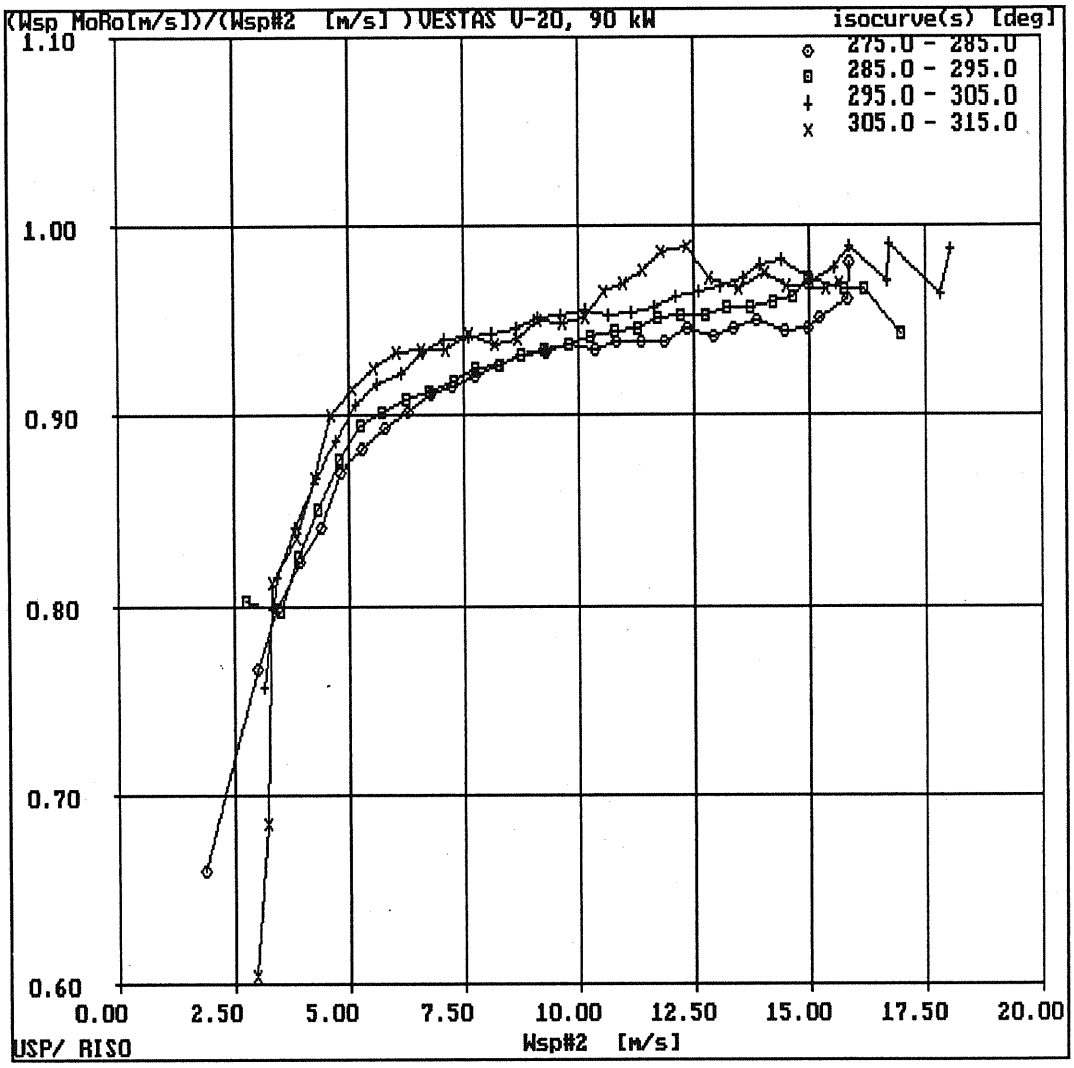

Fig.4.4.3. Wind speed deficit, mast -0.68D.

The anemometer responds with a wind speed less than virtual wind speed obtained at 2.5 rotor diameters ahead of the rotor. At the optimum rotor efficiency about 7.5% of the wind speed is lost.

The measurements of the velocity ratios obtained with different anemometer positions show a similar relationship when plotted against electrical power of the wind turbine, since electrical power is correlated with wind speed.

At the optimum rotor efficiency, a 1.6% axial wind speed reduction at -1.25D will increase C_E with 5%. At the anemometer position of -0.68D, C_E-max will be increased about 26%.

The flow field in front of the turbine has been shown to be distorted by the presence of the rotor. If we analyze the flow field behind the turbine, we expect a significant velocity decrease across the rotor plane. The wind speed at +1.50D relative to the upstream wind speed at -2.50D is shown in Fig. 4.4.4.

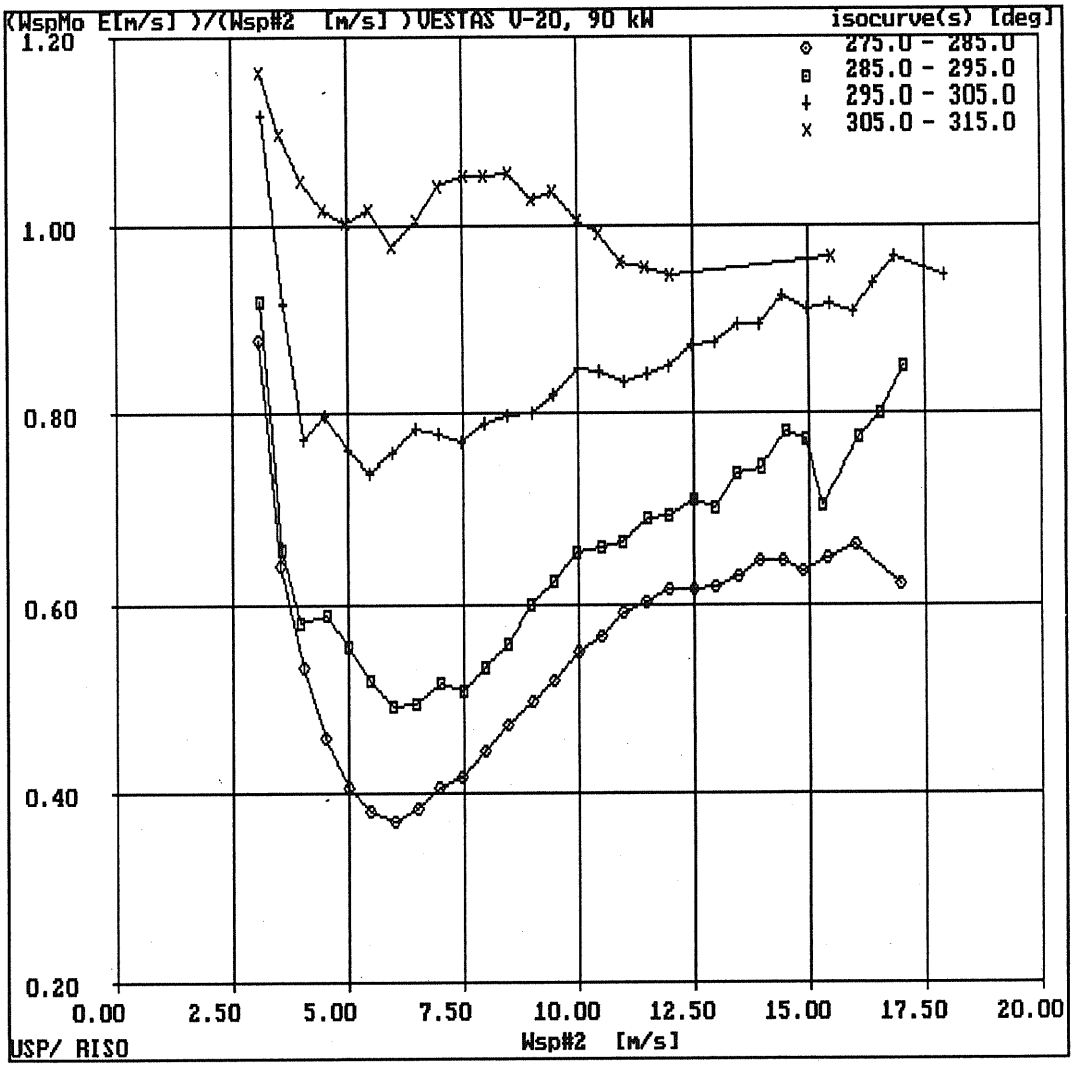

Fig. 4.4.4. Velocity deficit in the wake, mast 1.50D.

As expected the relationship is sensitive to the wind direction shifts, and the plot demonstrates the fundamental difference of the wake structure. The measurements are analyzed in the direction of about 285° centerline (line of velocity deficit) and for sectors of 295°-315°, where the anemometer is placed in the mixing layer of the wake and free stream flow field.

In the direction of 285°, axial wind speed is measured by the anemometer. Wind speeds between 4.5 and 7.5 m/s are reduced with 65% indicating that maximum power is extracted about 6 m/s.

The velocity profiles of the wake are shown in Fig. 4.4.5.

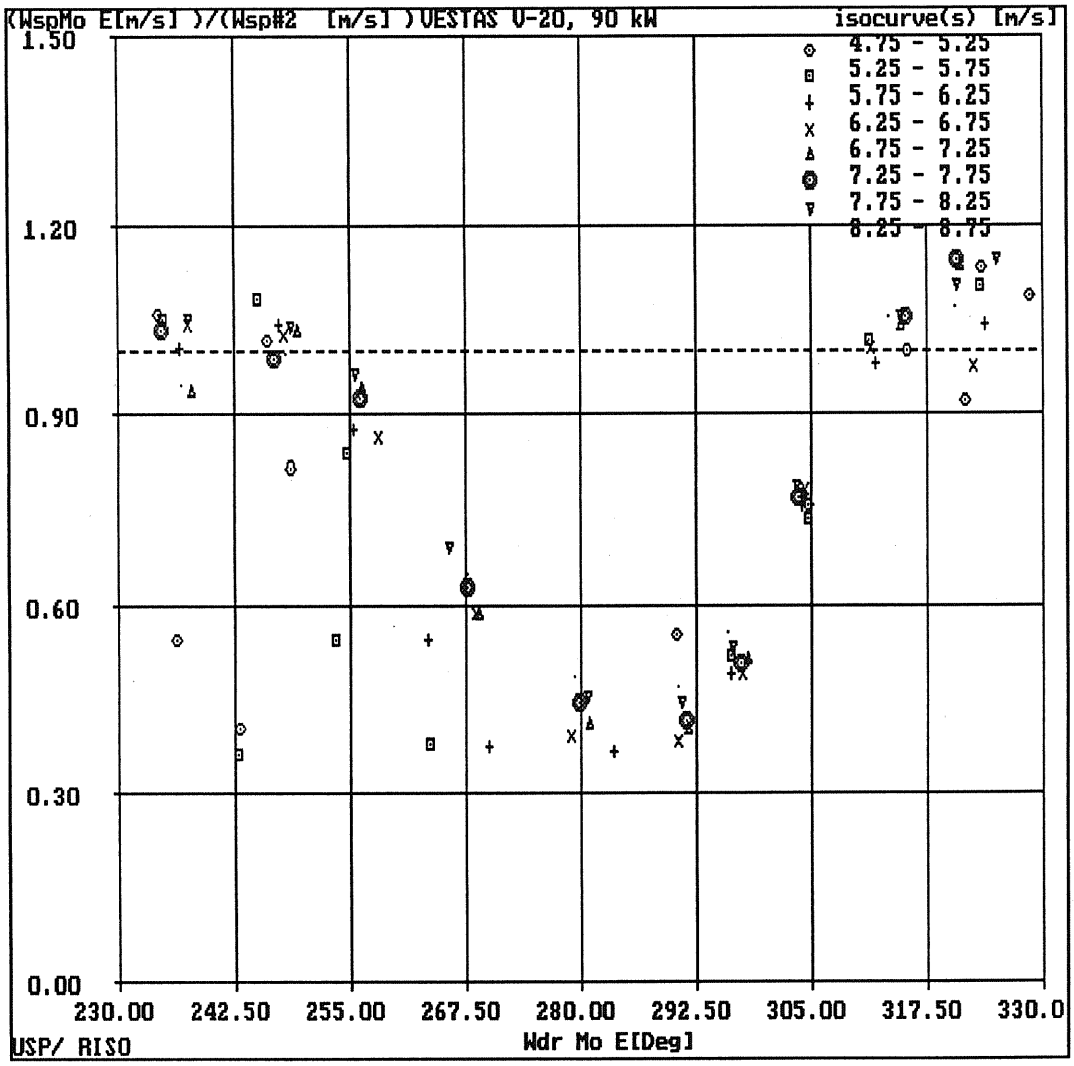

Fig. 4.4.5. Velocity profiles of the wake, mast +1.50D.

The plot demonstrate the symmetry of the bell-shaped curves with a global minimum of 0.4·WSP#2. It is also verified that the maximum velocity deficit coincides with the direction of 285°.

The broadness of the curve, which extends from roughly 243° to 318° indicates an approximate wake expansion of 66 m at the anemometer position.

5. COMPARISON BETWEEN FLOW MODEL AND MEASUREMENTS

A comparison between theory and measurements is made for anemometers arranged in the E-W direction in order to validate the theory involved. The model enables to calculate the local velocities around the wind turbine, and consequently to present a relationship between indicated and true wind speed at a reference mast. The model consists of two independently acting actuators in axisymmetrical flow. One is obtained from the induced flow of a semi-infinite vortex ring with constant diameter and the second from the multiple streamtube analysis combined with blade element theory (BET). The power calculation was presented in chapter 2.5.

5.1 The Flow at Optimum Rotor Efficiency.

Local velocities at mast positions of -2.50D, -1.25D, -0.68D and 1.50D are calculated at different onset wind speeds V_∞. The simplified vortex calculation method is used, formally identified by equations (1) and (2) presented in the annex.

At wind speeds below optimum rotor efficiency, the helical vortex sheets in the wake induce significant velocities at a blade element. Additionally the wind turbine operates in the vortex-ring state causing a non-parabolic relationship of local C_T vs. the axial interference factor **a** in the streamtube (**a** >= 0.5).

In order to take account of the corrections involved, the local axial induction factors found with the code ADYN_4 are averaged over the rotor disc. The average interference factor is then used as input for the simplified vortex model.

The local wind speeds, rotor efficiency and average interference factor are listed in Table 5.1.1. The wind speed range covers the optimum rotor efficiency. The figures in the brackets indicate measured wind speeds. Shear flow, tilt and yaw error influence will tend to decrease axial interference and consequently decrease the wind speed reductions shown.

Onset	Local axial wind speed					C_P	<a>
[m/s]	[m/s]						
V_∞	$V_{-2.50D}$	$V_{-1.25D}$		$V_{-0.68D}$		$V_{1.50D}$		
6	5.949	5.811	(5.9)	5.487	(5.4)	0.856	0.43	0.44
7	6.950	6.815	(6.9)	6.497	(6.4)	1.953	0.45	0.37
8	7.953	7.828	(7.9)	7.534	(7.4)	3.323	0.43	0.30
9	8.956	8.839	(8.9)	8.569	(8.4)	4.616	0.39	0.25
10	9.959	9.850	(10.0)	9.592	(9.4)	5.908	0.39	0.21

Table 5.1.1 Local axial wind speeds at optimum rotor efficiency.

A graphical interpretation of axial wind speed deficit is provided in the following plots.

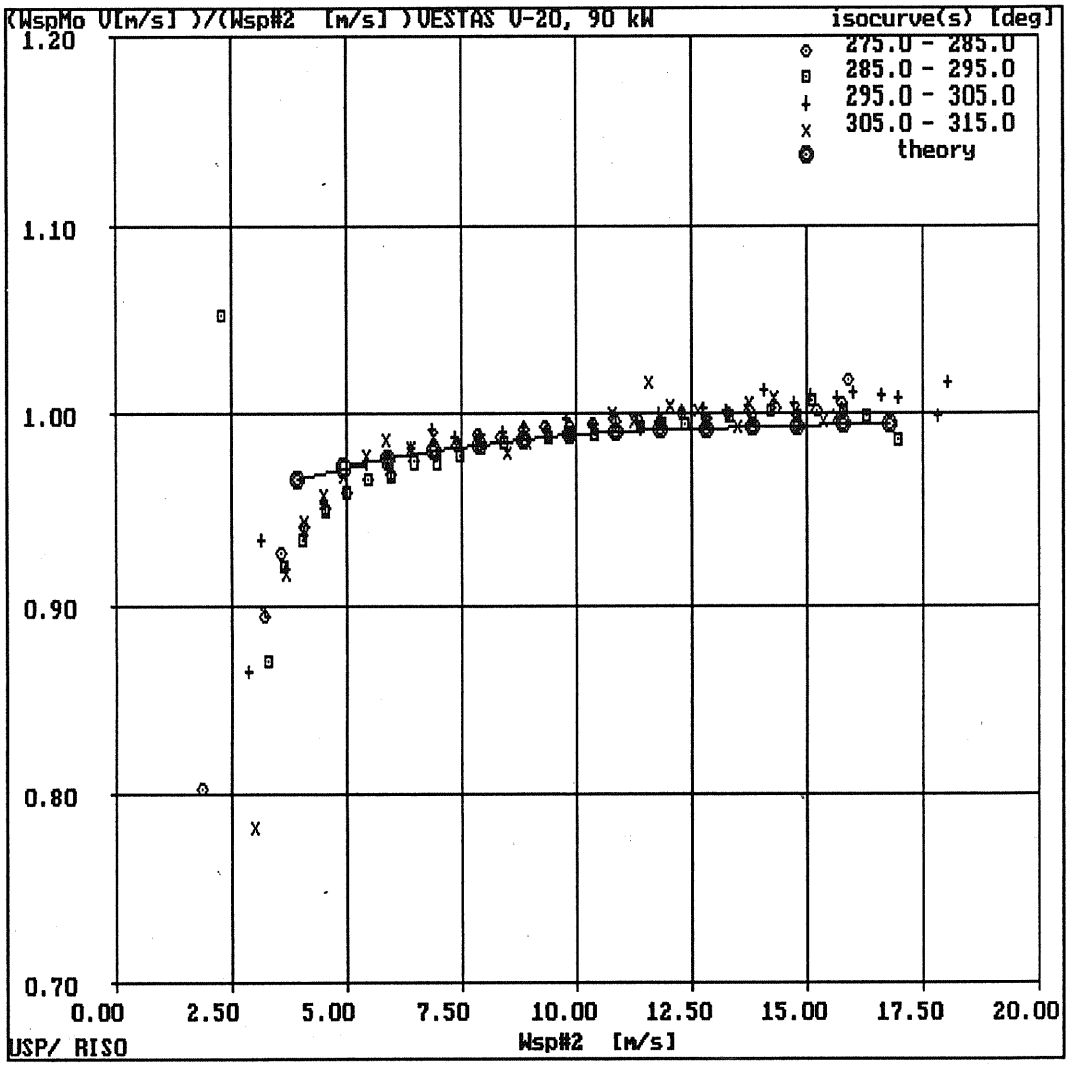

Fig. 5.1.1. Velocity deficit compared with theory, mast -1.25D.

The calculations conduct results very similar to measurements obtained at mobile mast 25 m in front of the turbine. The plot demonstrate that rotor disc interference is underestimated at wind speeds below cut-in condition of the turbine. <a> has to be increased with 90 % at 4 m/s and amplified 35 % at 5 m/s in order to match the average wind speed reduction in front of the rotor. Using this interference factor to calculate local wind speed in the wake will amplify the magnitudes shown in Fig. 5.1.3. significantly. This demonstrates that the BET and vortex calculation models have to be combined in adequate flow modelling.

Comparison of data obtained at mast position -0.68D with theory conduct an underestimation of non-dimensional wind speed with 2.5% in the measured wind speed range, as shown in Fig.5.1.2. Axial interference should be increased with 35 % in order to fit the experimental data.

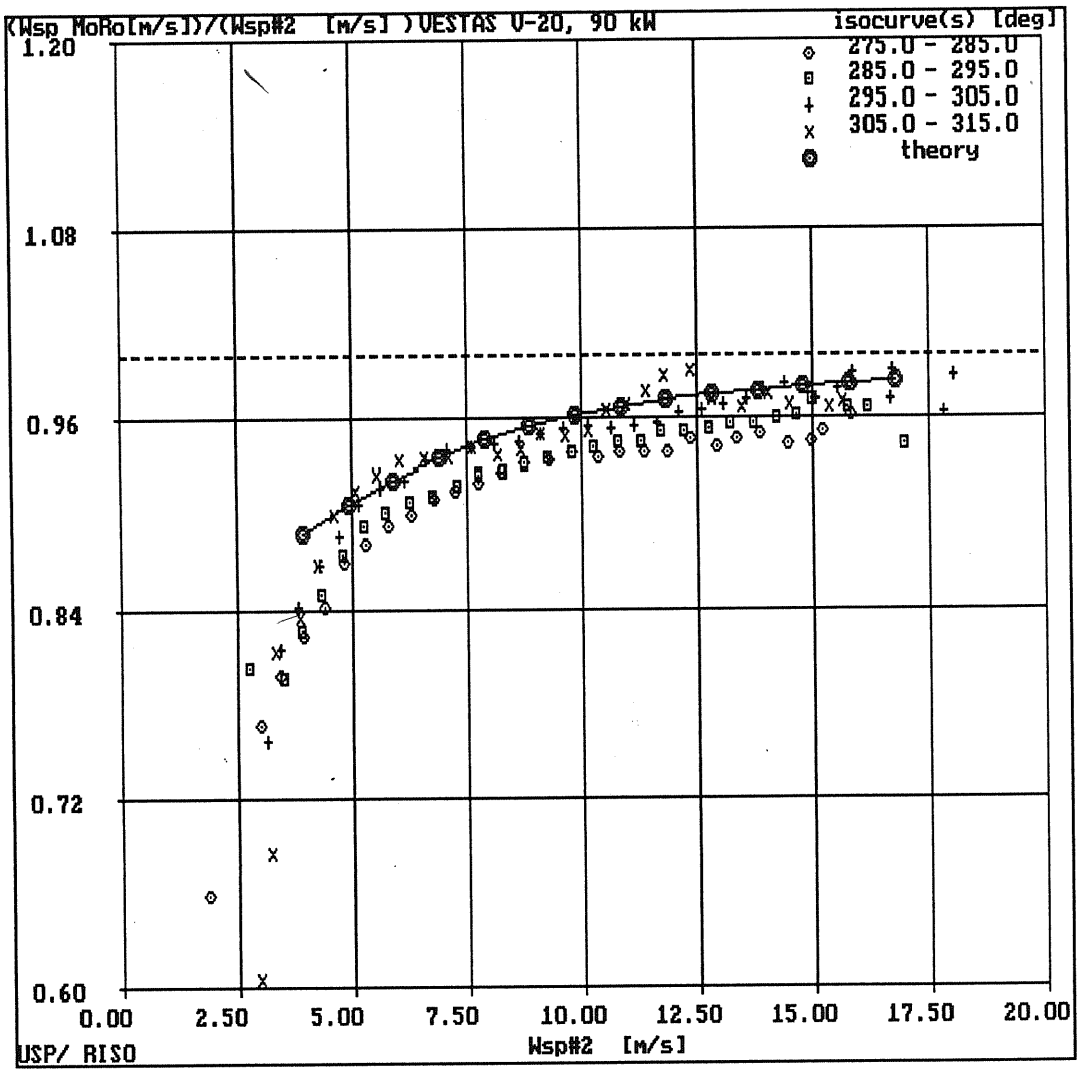

Fig. 5.1.2. Velocity deficit compared with theory, mast - 0.68D.

The model is restricted to the vortex filaments describing a cylindrical and semi-infinite rigid wake in a uniform onset flow. This assumption is obviously not adequate close to the rotor, where an expansion of the streamlines implies a displacement of vortex filaments in radial position and consequently an increase of induced velocities as indicated from experimental data.

Finally a comparison of velocities in the wake are made as shown in Fig. 5.1.3.

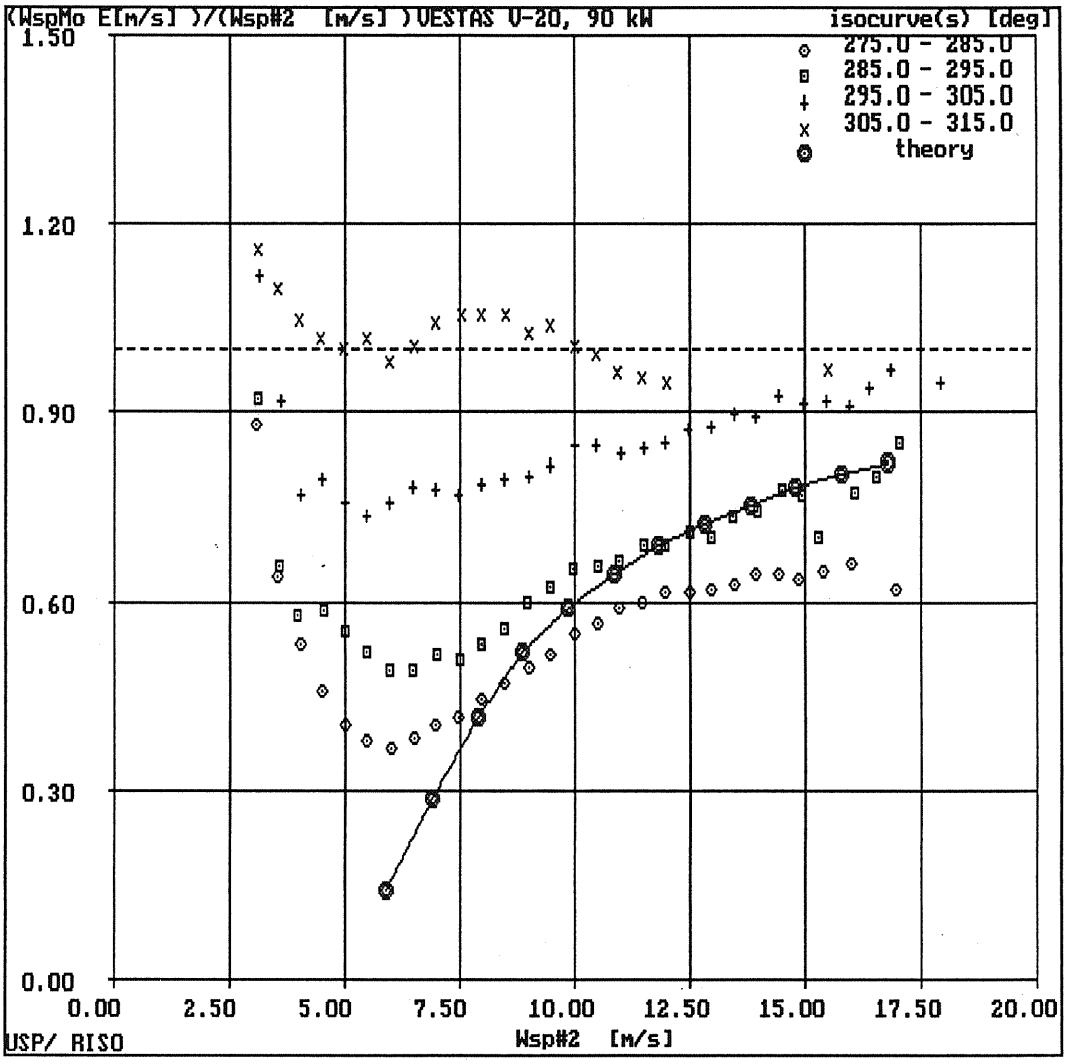

Fig. 5.1.3. Velocity deficit in the wake compared with theory, mast +1.50D.

The plot demonstrate a good correlation between the model and measurements for wind speeds above 11 m/s. For wind speeds below 11 m/s, the model overestimate the velocity perturbation of the wake. However, going to the limit of small wind speeds with the rotor stopped, the velocity deficit should be close to unity.

The interference factor can be deduced from measurements of the wind speeds just in front of and behind the rotor. At wind speeds about 6-7.5 m/s the velocity deficit accounts for 60% whereas the interference in front of the turbine approximately reduces wind speed with 7-8%. Interpolating to the rotor disc velocity the interference factor **a** is calculated to 0.34, which is about 10% lower than calculated with the code.

Summarizing the above experience, theory yields predictions within 3% (or $\sigma V_{50\,m} \approx 0.1$ m/s at $\langle V_{50\,m} \rangle \approx 7$ m/s) of the measured velocity deficits at the upstream positions on the centerline of the wind turbine rotor. Significant deviations between theory and experiment are obtained at mast positions just in front of and behind the wind turbine.

The theory tends to underestimate the induction from vortices at the upstream positions close to the rotor disc. It is evident that the wake modelling in this case is not adequately described for wind speeds below optimum rotor efficiency. Heavy disc loadings and consequently non-linear spacing of ring vortices occur in this case. The model do not account for yaw errors or rotor tilt influence, which tends to reduce the influence shown.

It is emphasized that the present modelling of the flow field in front of a wind turbine is sufficiently accurate for distances greater than 1.5D, which means that centerline axial wind speed deficit is proportional to $\langle \mathbf{a} \rangle_{uniform}$ and proportional to $(x/R) \cdot \{\sqrt{(1+(x/R)^2)}\}^{-1}$ to a first order approximation.

However, future work on theoretical modelling should take account of the interplay between rotor and wake calculations.

5.2 Recommendations for Anemometer Placement.

In order to stipulate the systematic error when measuring wind speed in front of a wind turbine in homogeneous flow, we resort to conditions of optimum rotor efficiency with a cylindrical vortex structure. Results are presented for the V20 HAWT assuming an axial interference factor of 0.37 at the condition of optimum rotor efficiency.

Calculations of induced velocities at different centerline distances in axial direction are conducted with the above formula, which are plotted in Fig 5.2.1.

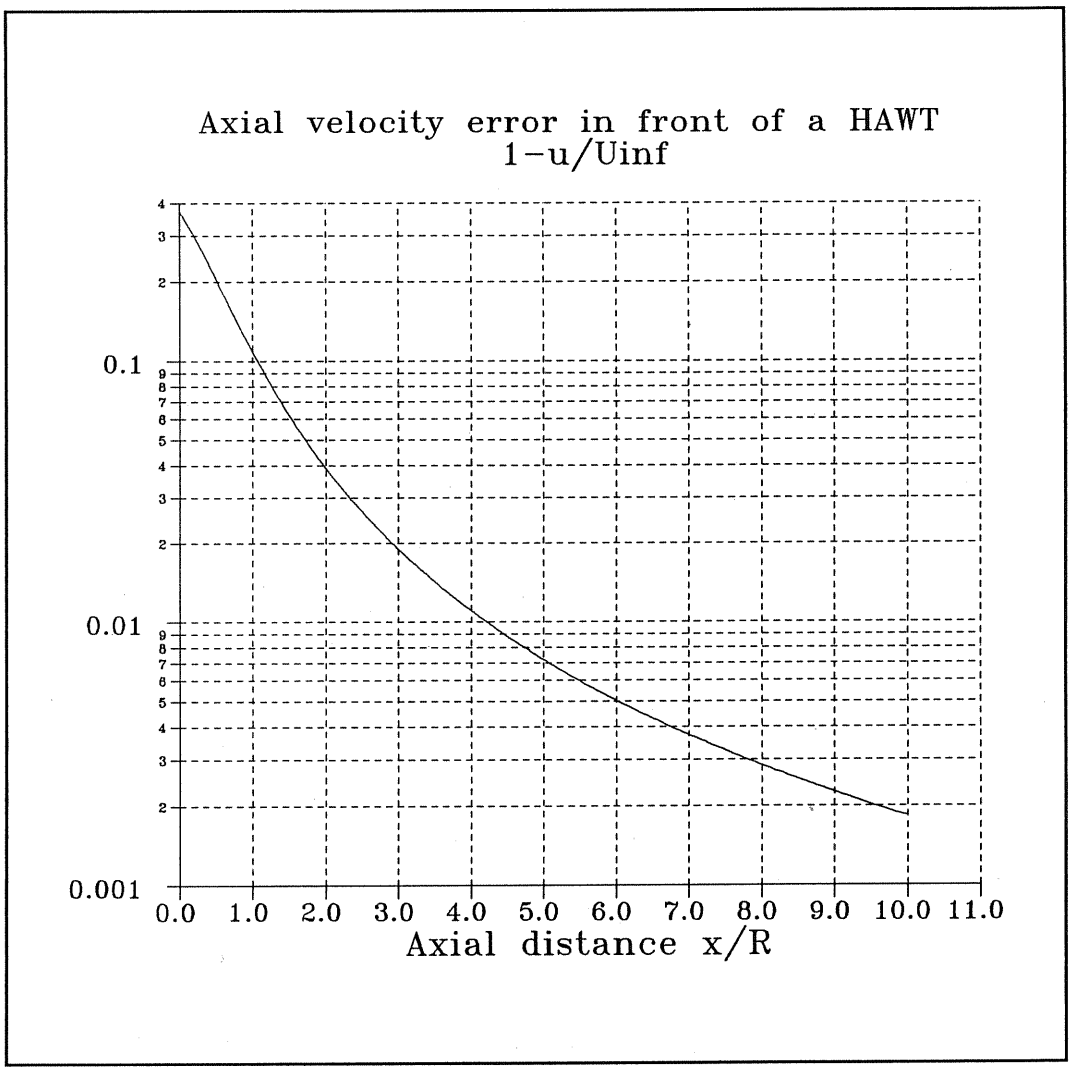

Fig. 5.2.1. Wind speed error vs. axial distances, R = 10 m

It is emphasized that a wind speed error of approx. 0.7% is obtained at a distance of 2.5 rotordiameters. The uncertainty of wind speed is then 0.07 m/s, which is in the order of accuracy obtained with a cup anemometer as the measuring device. However, international work within the CEC on cup anemometer calibration [6] and on wind turbine performance determination [7] recommend an instrument with an uncertainty better than a standard deviation of 0.1 m/s on mean wind speed. The IEA recommendation advise 0.2 m/s [2].

Although the bounds for accuracy seems to be fullfilled, progres in cup anemometer calibration tends to decrease the uncertainty on wind speed anemometers. It seems therefore plausible to advice the anemometer to be located at a distance of at least 3.5 rotordiameters in front of the turbine. This assures that the interference will be half as much as the figure obtained under present conditions.

The influence of terrain counteracts the placement of anemometers as correlation increases towards the rotor. The power scatter presented in this report deduce a separation distance under optimum conditions about 25 m (or 1.25 times the rotordiameter), a result which has to be combined with the distance of 3.5 rotordiameters. An adequate frequency domain model, describing the interplay between stochastic winds (as a point measurement) and dynamics of the turbine, could represent a helpfull tool in the finding of the optimum separation distance. The comparison between measurements and such a freqency domain model conducts comparative figures of power scatter within a bin in lateral direction (see chapter 4.2).

5.3 Proposals for Additional Work.

Concerning power curve determination, analysis of statistical properties of the energy capture for a HAWT should be initiated in order to elucidate figures like turbulence, power varibiality and $\sigma P/\sigma V$.

One of the results of the present investigation demonstrated the influence of terrain effects at the site, which could be analysed intensively with Wasp code (Sensitivity of results due to geometrical inputs, test of accuracy of model).

A major progres could be made by adjustment of meteo mast intercalibrations made on the basis of measurements on the terrain effect(wind speeds between 4 and 20 m/s, proper data representation at 6 - 8 m/s for conditions of optimum rotor efficiency).

Close to the rotor disc, the upstream flow should be modelled more adequately in order to improve comparison between measurements and theory predicting local flow velocity.

6. CONCLUSION

The present report describes aspects of flow and power performance on a horizontal axis turbine of make Vestas, 100 kW.

Investigations of the terrain effect on the power curve measurements demonstrates the complexity of the parameters involved and their influence on the power quality in terms of the scatter, the turbulence and the directional variability. Additional measurements on the terrain effect is recommended in order to improve interpretation of the present findings.

One major source for power curve fluctuations is the turbulence induced by neighboring, operational turbines.

The report concludes, that the scatter on the electrical power is reduced for anemometer placed closer to the disc, but to the expense of increased turbulence.

The measurements carried out and analyzed indicate the need for taking the wind speed retardation into account in front of a turbine.

Application of the vortex theory assuming a rigid wake structure conduct velocity deficits less than 3 pct of the observed wind speed reductions. The velocity deficit is not predicted adequately at low wind speeds. This happens especially in the wake, which might be a consequence of decoupling the rotor and wake calculations.

The comparison between the theory and the experiments demonstrates the need for correct anemometer placement at an upstream condition, which is practically unaffected by the presence of the rotor. Irrespective of space correlation between rotor power and wind speed, a placement at 3.5 rotordiameters would imply a 50 % reduction of the error on wind speed due to flow stagnation. The shortcomming of reduced correlation has to be considered.

REFERENCES

Ref. 1 Wind Turbine Test Vestas V20, 100 kW.
Uwe Schmidt Paulsen, Søren Markkilde Petersen, Per Vølund, Troels Friis Pedersen. Risø M-2709.

Ref. 2 Recommended Practices for Wind Turbine Testing and Evaluation, Part 1: "Power Performance Testing" IEA recommendation edited by
S. Frandsen, A. Trenka and B.M. Pedersen

Ref. 3 Accuracy of Power Curve Measurements .
Editors C.J. Christensen & J. Dragt. Risø M-2632

Ref. 4 Aerodynamics of a Full-scale, Non Rotating Wind Turbine Blade under Natural Wind Conditions.
Uwe Schmidt Paulsen. Risø M-2768

Ref. 5 N.O.Jensen, Risø. Private communication.

Ref. 6 The Accuracy of Cup Anemometry with specific regard to Calibration Technique and Overspeeding. Report No.EUEC/25;ECNL/03. NEL Jan. 1989.

Ref. 7 Recommendations for a European Wind Turbine Standard on Performance Determination.
A. Curvers, ECN and T.F. Pedersen, Risø. Report ECN-217 July 1989.

ANNEX

LITERATURE SURVEY
ON
FLOW EFFECTS FOR HAWT

SYNOPSIS

At The Test Station for Wind Turbines measurements on electrical power and wind speed have been carried out in order to investigate the influence from natural wind on the measurement conditions. The aim of the project is to clarify the sensitivity on power curve evaluation due to anemometer setting, block averaging time, influence from the landscape and the distortion of the windfield caused by the presence of the wake from the wind turbine.

A review of literature issued on the flow field for HAWT & VAWT rotors is performed. Special attention is put on factors influencing the flow in front of a horizontal wind turbine.

INTRODUCTION

The discussion of power curve measurements has given attention on possible errors influencing the power curve estimation.

The power curve evaluation has been performed on the basis of IEA recommendation (Ref.1).

Field measurements (Ref.2) performed within IEA power curve recommendations indicate a possible flow influence on a cup anemometer placed at 2.0 rotor diameters in front of the WEC. The influence of the wake from the wind turbine might cause a retardation of the windfield in front of the WEC at the position of the anemometer.

The particular observation has been disregarded until recently because the influence of the wake has been assumed to be negligible at distances greater than 2 rotor diameters.

REVIEW OF RELATED WORKS ON THE SUBJECT

1. Theoretical work

Flow field calculations are divided into different types of flow models. The subject is discussed relative to vertical axis wind turbines by a number of authors, see for instance O.de Vries (Ref.3), H.A. Madsen (Ref.4) and Paulsen et al (Ref.5).

Different concept are discussed in Ref.3, valid for both HAWT & VAWT turbines. The flow models are divided into kinematic and dynamic models. The kinematic models are based on vortex flow models or differential equations describing the flow (Euler equations, Navier Stokes equations). Both steady and unsteady flows can be treated. In Ref.5 a free wake, unsteady analysis is performed on a Darrieus Wind turbine.

The other main part of flow models is based on the concept of describing average quantities (steady flow) from a streamtube

model. The formulation of streamtube concept is closely related to the use of actuator disc(s).

The basic formulation of streamtube models is described in (Ref.3.) with the momentum theorem. The model is not able to predict the windfield in front of and behind the rotor, but it is a powerful tool of estimating performance at high tip speed ratios.

Actuator disc theory in differential application yields calculations of induced wind speeds, see (Ref.4.).

The combination of the Euler equations together with continuity of mass yields a Poisson type equation and with proper boundary conditions, the equation can be integrated. In Ref. 4 the velocity on the centerline for a actuator disc is computed. The result is reviewed in Fig. 1.

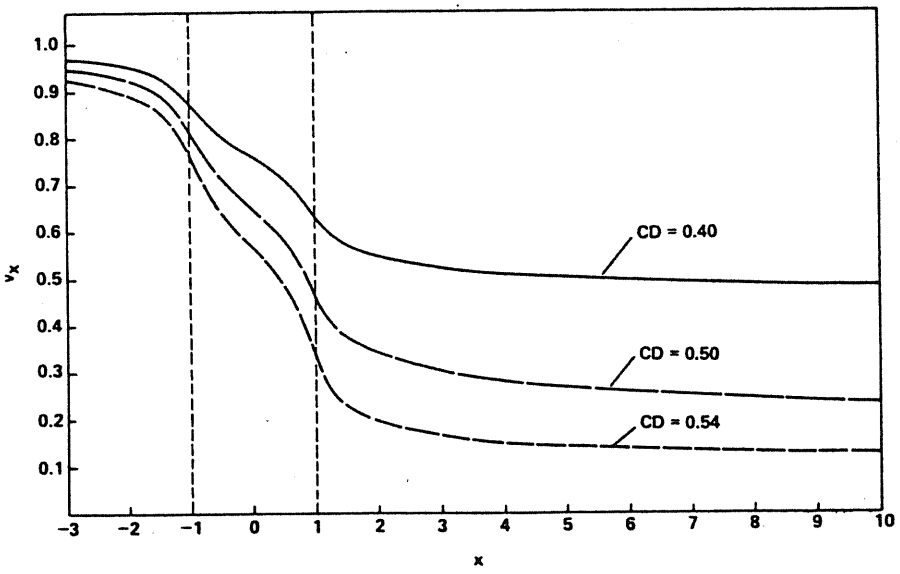

Fig.1. Velocity component in the centerline direction at different loadings. From Ref. 4.

The figure indicate at upstream locations disturbances in the range of 5- 10 % of the onset flow.

A comparison can be made with the finding of Zervos at al Ref. 6. They use vortex theory as described in Ref. 5.

Windfield calculation 1 rotor diameter ahead of the 2 bladed turbine with pitch angle and solidity 0.180 is shown in the following plot.

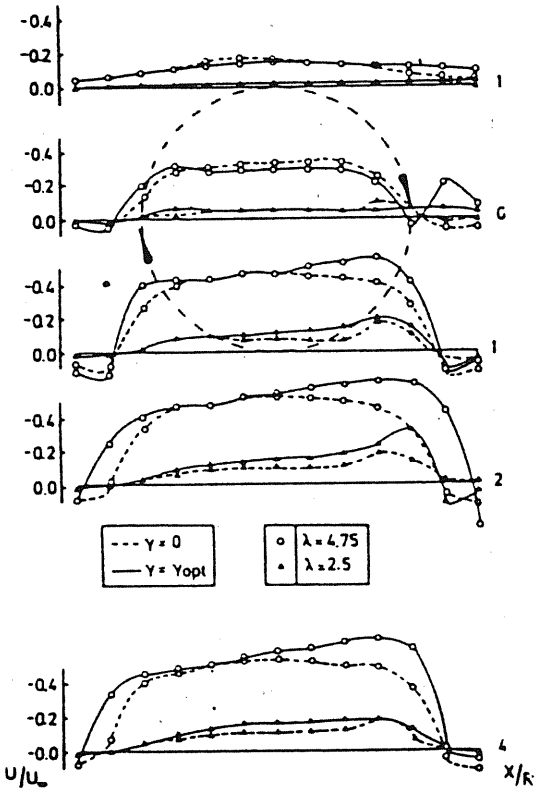

Fig. 2. Induced velocities at various sections. From Ref. 6.

The main result of these findings indicates that flow retardation increases for larger tip speed ratios. The flow effects are limited to 5 - 10% at 3 rotor diameters, which is 0.5 - 1 m/s at an onset wind speed of 10 m/s.

In relation to HAWT application, the induced velocities have to be reduced in magnitude and direction. The swirl in front of a HAWT rotor is considerable lower than from VAWT conditions. Van Briel et al (Ref. 7.) investigated 2 dimensional flow of a HAWT by means of momentum theory in a rotating frame of reference. They found the flow to diverge continuously in a helical manner with diminishing pitch. At a loading comparable with an axial induction factor of 0.5, the swirl angle in the rotor plane is 3.4 Deg at a tip speed ratio of 8.5.

Momentum theory predicts the velocity field in the disc, and is not able to predict the flow field between the locations at the actuator and at infinity at upstream location. Since no mechanical work is performed on the flow between these stations, angular momentum and total entalpy have to be constant.
(Assuming non-expanding streamtubes, $V_0 r$=constant will be obtained with V_0 as tangential velocity at the radial position r).

The tangential velocity contribution is of central interest, because it identifies the total induced velocity at the actuator (Ref.3).

The discussion of theoretical HAWT flow models has been applied by O. de Vries (Ref.3). Although theory was developed in the 20'ties and 30'ties, powerful computational methods of potential theory (as described above) becomes operational with more powerful computers. Use of this theory has been made by M.B. Anderson (Ref.8).

Vortex theory is modeled with tip and root vortices and compared with conventional momentum theory, modified with Goldstein's approach for tip loss estimation.

The author concludes, that discrepancy exist in flow situations determined by back-flow (windmill brake situation), but obviously these errors are small on the loads and performance.

The author finds considerable deviation between induced velocities, when calculation is performed with a rigid wake model and with a force free representation of the vortices (free wake analysis). That means, that vortices should obey kinematic relations allowing the vortices to drift with the local velocity. The tangential velocity component along the tip vortex in the wake is not changed drastically as the radial and axial velocities. Furthermore it determines extracted power through the Euler turbine equation.

The application of vortex theory determines the flow field at every location. A simple flow field model for HAWT is given by R.E. Wilson (Ref.9.). The author uses actuator disc theory to compute the mean axial velocity at the disc and superimposes induced velocity components by application of the Biot-Savart Law.

The wake is assumed to consist of a cylindrical vortex sheet with constant diameter 2R (analog to an electromagnetic Solenoid device).

The axial component u at the distance x is reproduced here as:

(1) $u/c_0 = 1-\mathbf{a}\cdot(1+ X/\sqrt{[1+X^2]})$

$\mathbf{a}$ is the axial induction factor

c_0 is the onset velocity

X is equal to x/r

The continuity equation yields radial velocity v as:

(2) $v/c_0 = 0.5\cdot\mathbf{a}\cdot Y/\sqrt{[1+X^2]^3}$, $Y = y/R$

In the free wake analysis, radial flow velocity vary linearly with radial position (Ref.9.).

H.A. Madsen (Ref. 10.) made simplifications on this actuator disc model (Ref.3.). Neglecting transverse body forces he ended up with an analytic relation between velocities, position and load. However, the 2-dimensional, semi-infinite disc application is valid for drag-coefficients less than 0.3 (x positive down stream). The velocities can be deduced as:

$$(3) \qquad u/c_0 = 1-C_T \cdot [\mathrm{Atan}(1-Y)/X)+\mathrm{Atan}((1+Y)/X)]/4\pi$$

$$(4) \qquad v/c_0 = \tfrac{1}{2} \cdot C_T \cdot \ln[(X^2+(Y+1)^2)/(X^2+(Y-1)^2]/4\pi$$

C_T is conventionally related to the slowdown factor a by

$$(5) \qquad C_T = 4\mathbf{a}(1-\mathbf{a}) \ , \quad \mathbf{a} < 0.5$$

Situations of **a** >= 0.5 occur in the windmill-brake state.

At an axial distance of x/R = -4 with **a** $\approx$ 0.0817 (yielding $C_T \approx 0.3$), equation (1,2) yield $u/c_0 = 0.9976$ and v = 0 and Equation (3,4) $u/c_0 = 0.9883$, v = 0.

The difference between these two flow models is about 1% in axial direction and a calculation on crosswise flow yields at Y = 1 a deviation of 22%. Due to the semi-infinite vortex filament described by the equations (3,4), induced velocities are higher in the case of axisymmetrical flow.

Küchemann (Ref. 11.) has tabulated induction factors for vortex ring application. These factors are evaluated on the basis of the Biot-Savart Law. He notices, that the general flow can be resolved by obtaining the streamlines for an approximately vortex shape. The vortex cylinder would represent the first approximation and streamlines could be obtained. With the given vortex distribution arranged on the deduced vortex shape, further approximately solutions can be obtained. Fig. 3 comprises results taken from the reference with application on a cooler block (flow pattern are similar to those of a HAWT)

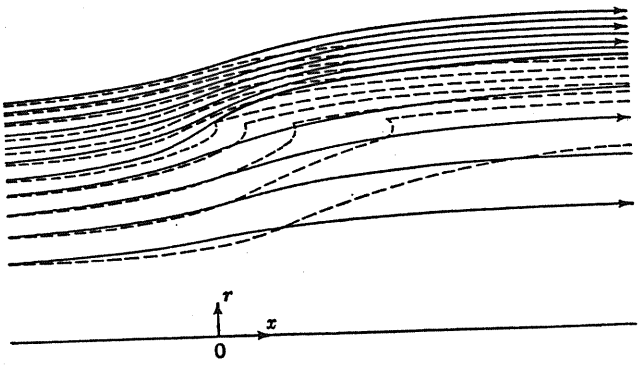

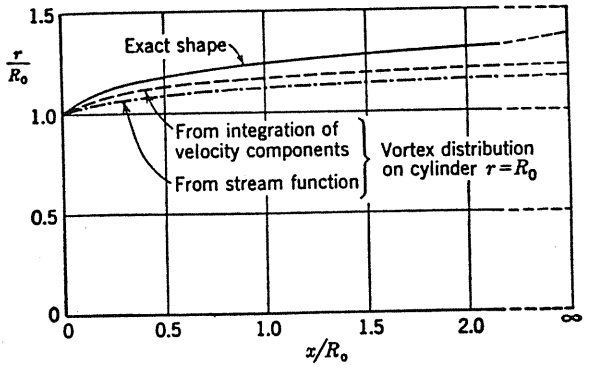

Fig. 3. Results from Ref. 11.

It is obvious, that the expansion of the wake will induce velocities exceeding those obtained from the induced windfield in the case of a cylindrical wake.

2 Wind tunnel and field measurements on flow effects

Flow retardation in front of a rotor has been considered by few authors. Most research has been practiced on the lee-side region in order to investigate turbulence phenomena in the wake region.

Some works are describing the flow field of VAWT's, see Michos et al (Ref. 12). In this reference several other authors are mentioned working with power performance and flow visualization.

Michos and his coworkers investigate the flow field both upstream and downstream of the rotor. At luv-distance of 0.55 rotor diameters they found a retardation of about 10% relative to onset flow (see figure 5). The turbulence intensity distribution is Gauss-shaped with max. intensity of about 6% at equatorial station. The 2-bladed model has a solidity of 0.159.

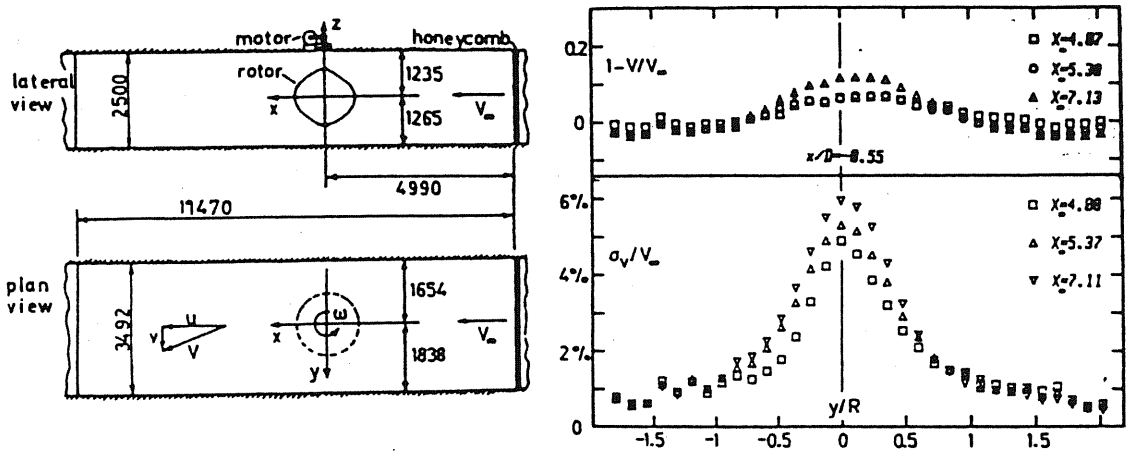

Fig. 4. Velocity and turbulence intensity distribution upstream of the rotor (from Ref. 12).

Wind tunnel investigation on a 3-bladed 2.64 m HAWT model has been carried out by A. Papaconstantino et al [Ref. 13.]

At upstream location (-R/2) they report a 4% retardation at the blade area. On the centerline at -R/6 and -R/4 the retardations approach 12%. The figures are valid for tip speed ratio of 6.

The flow deflection is reported to 1 Deg from the horizontal at -R/2. At -R/6 the deflection is reported to be 4 Deg.

Turbulence measured with the hot-wire was found to be 1%, which was the same as obtained in the empty tunnel. (tip speed ratio equals 4).

The wind tunnel blockage from the experiment is found to be 33%, which makes the measurements spectacular even with compensation for blockage effects.

Intensive work on windmill brake condition is performed by Ostowari and his co-workers. Their wind tunnel studies illuminate flow in the case of slowdown factors exceeding 0.5, wake expansion and tuft studies.

A study of non-uniform approach flow has been presented by M.A. Kotb et al (Ref. 14.).
They put different types of screens in a wind tunnel and measured velocity in the wake and power performance on a 3-blade, 0.49 diameter pitch-regulated model rotor. The upstream velocity distribution is modeled with a horizontal shear parameter of $R/c_0(Y=0) \cdot du/dy = 0.0802$ with $c_0(Y=0)$ as the mean center velocity and Y transverse coordinate with the highest velocity in the negative Y direction.

In the case of shear flow, maximum power coefficient decreased about 8% relative to uniform flow field case. The tip speed ratio was calculated to 3.06 with the centerline velocity in the denominator. The uniform flow was decelerated 60% at 35% from the radial position of the hub. At the tip region a small speed-up influence was reported.

Outside of the disc, velocity was unaffected form disturbances. In the case of shear flow, swirl just behind the disc was decreased to 8.5% velocity from 10% obtained with uniform flow. Furthermore, observations indicated that axial velocity deficit with uniform flow was higher than flow with shear profile.

Finally, upstream conditions were found not to influence radial velocity profiles.

Full scale measurements are available form Nibe HAWT made by. J. Højstrup (Ref. 15). Although most of his work describes wake conditions, some of the results are giving information on upstream flow conditions at 1 and 2.5 rotor diameters.

The velocity profiles are shown in Fig. 5 at a load of 77% and in Fig. 6 at a load of 20%.

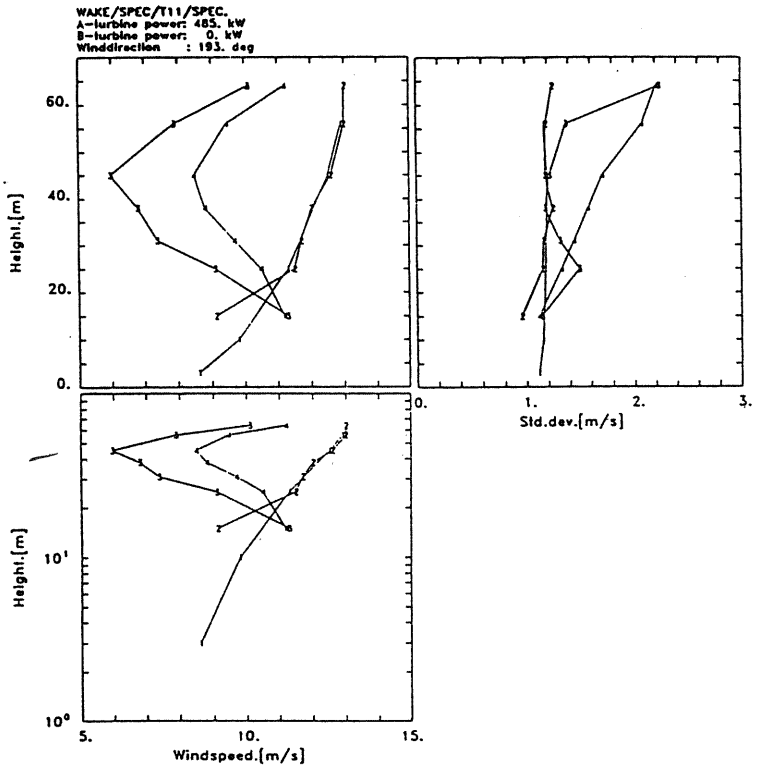

Profiles of mean wind speeds and standard deviations of wind speeds measured with cupanemometers. The standard deviations plotted represent half the variance to conform with the plotted spectra that integrate to half the total variance.

Fig. 5. From (Ref. 16)

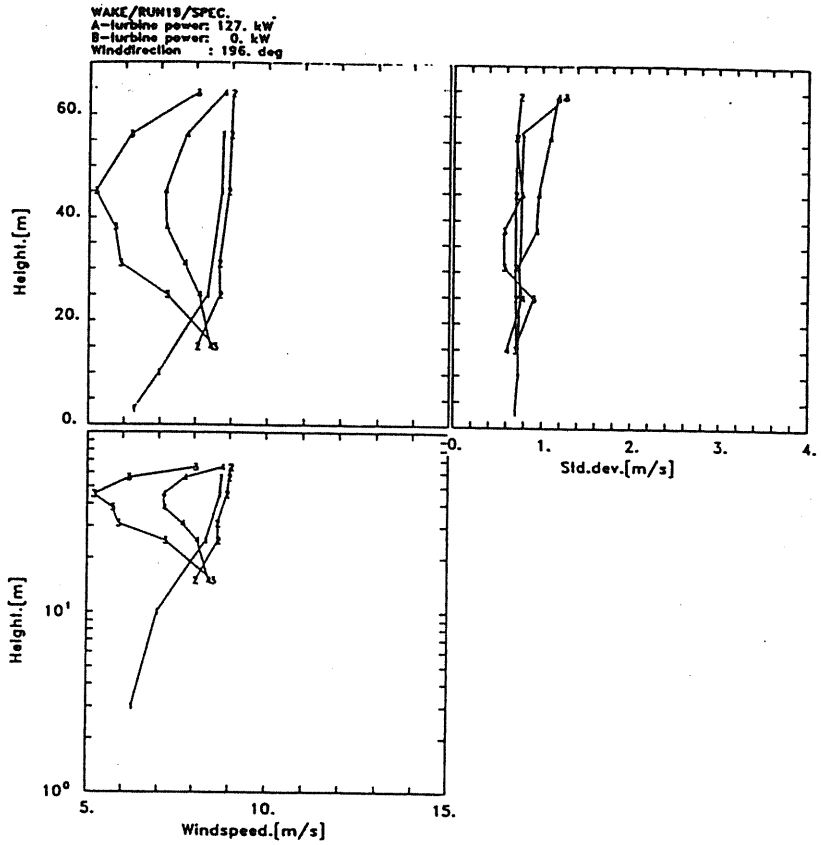

Fig. 6. Profiles of mean wind speeds and standard deviations of wind speeds measured with cupanemometers. The standard deviations plotted represent half the variance to conform with the plotted spectra that integrate to half the total variance. From (Ref 15)

The difference between measured wind speed at 1 rotor diameter and 2.5 rotor diameter is not significant in the case of high loading (low tip speed ratios relative to off-design).

At 20% load (high tip speed ratio relative to the off-design) a constant offset of about 0.2 m/s is measured. The standard deviation gives same information. The anemometer located close to the HAWT was reported to measure the smallest wind speed relative to wind speed measured at 2.5 rotor diameter upstream location. The influence of terrain is not obvious from these measurements. According to private discussion with Højstrup, 20% load case could refer to meteo unstable conditions, which is contrary to the case of fig. 5.

3. Related works describing combined/interrelated problems of measuring power curves.

Flow effects are interrelated to turbulence, caused by several mechanisms.

Atmospheric turbulence and fluctuating quantities (gust) in the boundary layer are major inputs to the HAWT. Manwell and Kirchhoff (Ref. 16.) considered the power available in turbulent wind and the ability of a HAWT to capture that power. The authors found, that the fraction of the additional energy available from turbulence fluctuations ranges between 3% and 37% and this contribution is more than would be predicted by hourly averaged wind speeds. For a constant speed rotating HAWT, approx. 70% of additional energy could be extracted. The idea is further pursued by H.G. Beyer & G. J. Gerdes (Ref. 17.) in their effort to calculate hourly mean power output in a real windfield. The analysis is carried out on a pitch regulated wind turbine and the major finding concludes a decrease of power output with increasing turbulence intensity.

The spectral analysis incorporated in the analysis has been extended to describe loads on HAWT's (see P.H. Madsen (Ref. 18)).

A somewhat different scope has been undertaken in the work of S. Frandsen (Ref.19.) discussing uncertainties in power performance measurements and by T.F. Pedersen et al (Ref. 20).

Frandsen discus several sources of errors influencing power performance measurements. Since power curves are evaluated through the method of bins analysis, the method implies additional error at a certain bin size. The author reviews the different aspects of this computational method.

Furthermore, attention is put on averaging time and on tracing the most correct block averaging time.

The time constants which determine averaging time are considered: length scale of turbulence, rotor response time and the separation of wind turbine and meteo tower.

For a more comprehensive discussion it is recommended to consult the reference. Discussion of coherence filter function determinating separation length between tower and wind turbine is performed by M.S. Courtney (Ref. 21).

However, Frandsen illustrates rotor filter and coherence function for a 20 m diameter HAWT, with the anemometer located 2 rotor diameter upstream of the machine. This relationship together with the sample averaging filter function of

$$F(n) = \sin^2(n\pi T_{ave})/(n\pi T_{ave})^2$$ with

T_{ave} as the sample averaging time and n as the frequency is shown in figure 8.

Drive train frequency response function, rotor averaging filter function, and coherence function for a 20-m-diameter rotor with the test anemometer two rotor diameters upwind. In addition, a "running average filter" is shown with a cut-off frequency of 1/30 Hz.

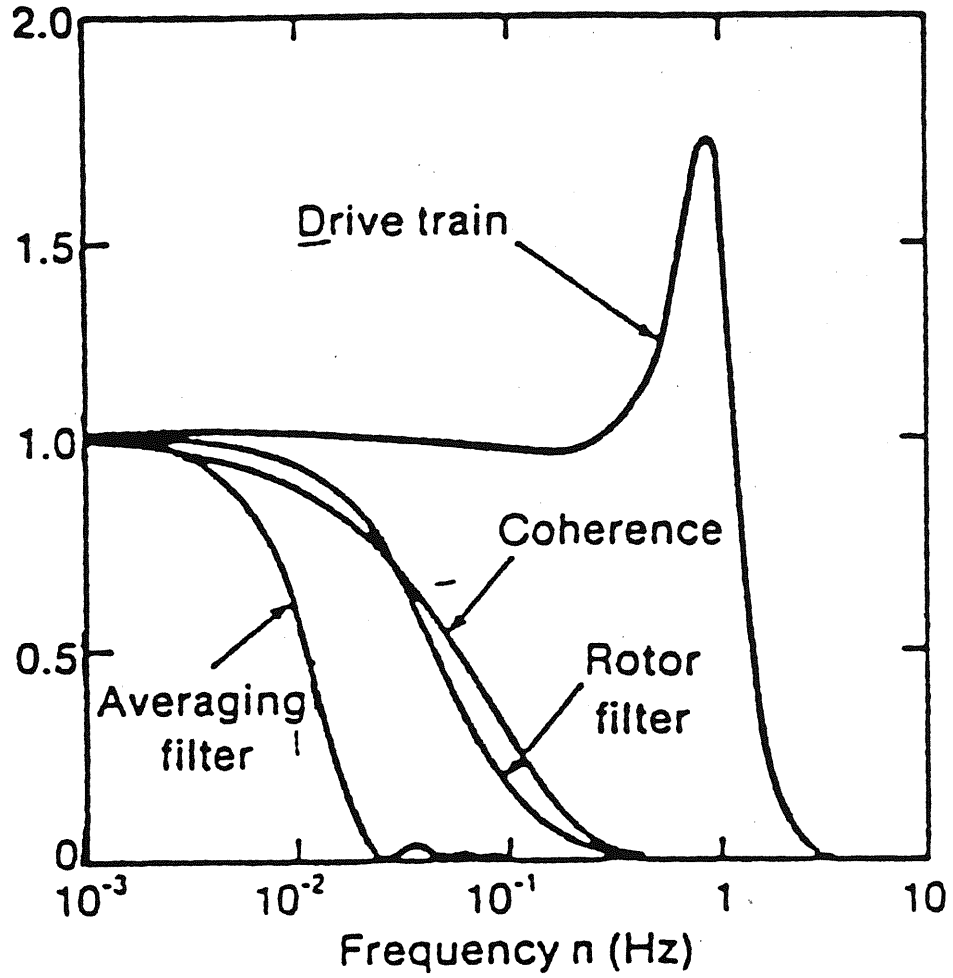

Fig. 7. from Ref. (20)

T.F. Pedersen et al (Ref. 20) analyzed power curves from a 90 kW V20 Vestas HAWT with a theoretical frequency domain model suggested by Christensen & Dragt (Ref. 22). They found from their model which bears analogy to the analysis of Frandsen, that the relative precession index

$$Si = \sigma P/\sqrt{n} = \sqrt{t/T}$$

is highly correlated with separation distance, wind flow direction relative to anemometer and wind turbine placement, and averaging time. Results are reviewed in fig. 8 and 9.

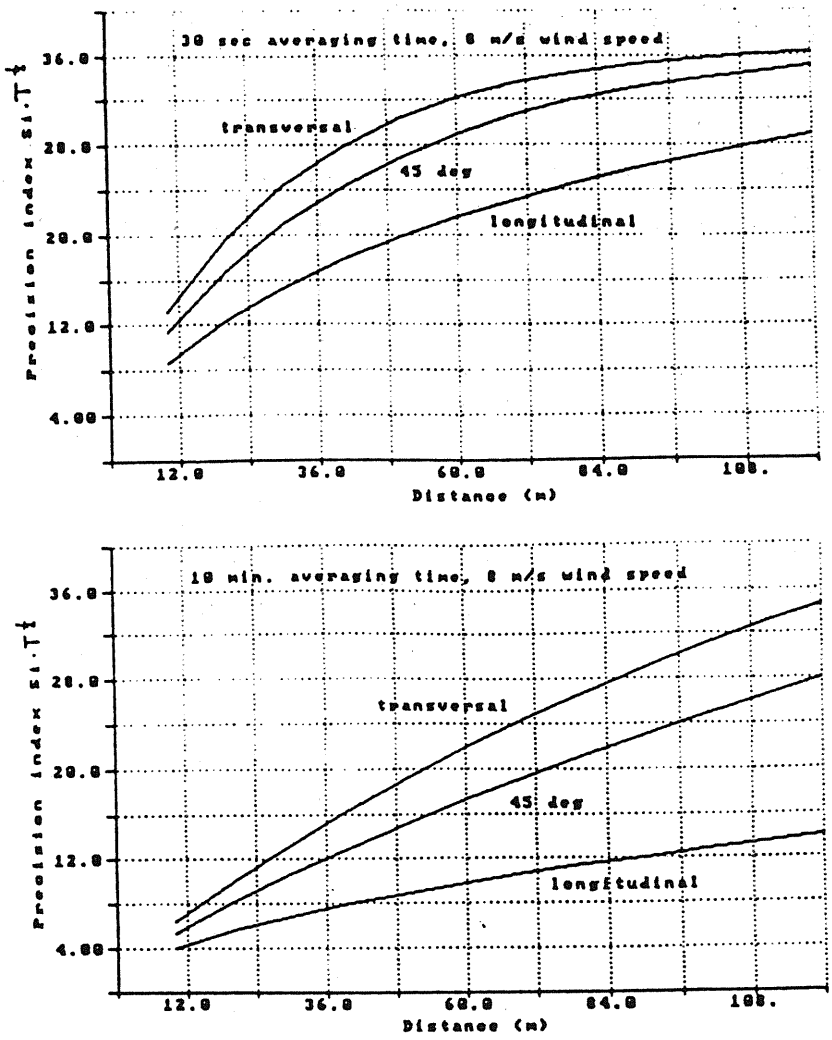

Fig. 8. Relative index as function of distance and direction to anemometer mast. From Ref. ~~20~~ 21

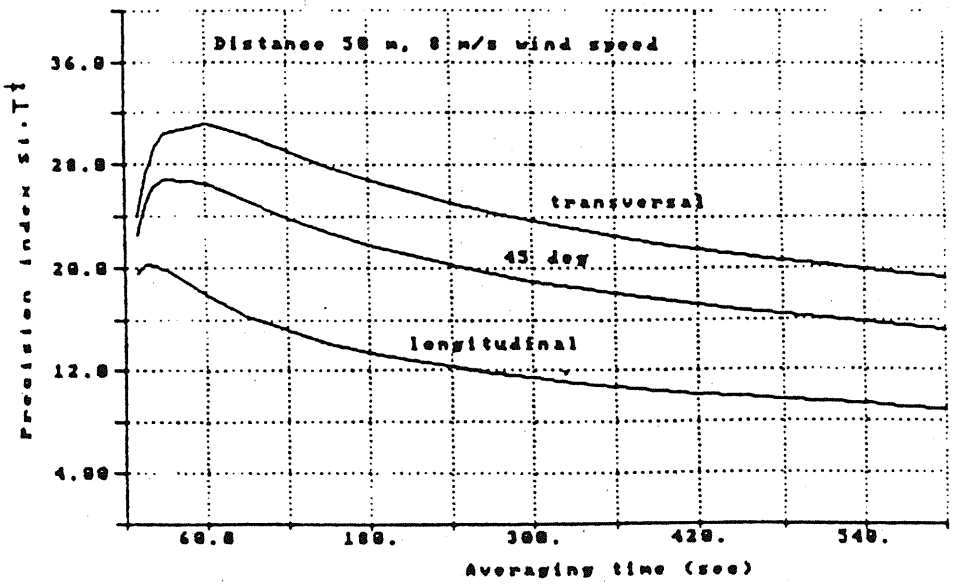

Relative precision index as function of averaging time.

Fig. 9.

From Ref. 21

The authors discus windfield influence on power performance measurements. They have noticed a 0.4 m/s overall reduction of wind speed on a cup anemometer located 0.65 rotor diameter ahead of the rotor relative to a anemometer, which is 2.5 rotor diameters upstream of the machine.

W.A. Vachon (Ref. 23) summarizes the significant sources of errors in estimating wind energy production. The author identifies following errors inherent in wind speed measurement: cluster effect, power curve, yaw angle deviations and wind turbine operational strategy.

The errors due to wind velocity measurement are identified through: calibration errors, bias and scale factor drift, mounting errors (inc. tower shadow) vane errors in case of propeller anemometer, bandwidth errors or lagging response, cup anemometer over speeding due to different time constants for speed-up and slow-down, sampling errors, flow field errors due to improper anemometer placement and inadequate coverage of the rotor swept area. Vachon demonstrate in his paper bandwidth errors due to different response of anemometer and wind turbine. The method is similar to that obtained from Frandsen. Finally, cup anemometer over speeding is investigated.

Finally, attention has been drawn on estimating turbulence. Numerical simulation of a 3-dimensional field of turbulent wind has been performed by P.S. Veers (Ref.24) for use in the aerodynamic and structural analysis of wind turbines. One of the findings confirms the results obtained from M.S. Courtney.

The estimation of turbulence variance and scale for wind turbine applications has been performed by D.C. Powell (Ref. 25). The author recommend that turbulence variance should take the form of :

$$\sigma^2 u = 1.2 \cdot [U(H)/\ln(z/z_0)]^2$$ with z as height parameter, z_0 as the surface roughness length.

The estimation of integral length scales are given. Theory predicts linear variation with height, whereas measurements indicate a linear relationship of height with integral length scale, powered with 5.

The author shows, that variability in integral length scales are obtained with different approach of data handling.

REFERENCES

REF. 1. Recommended Practices for Wind Turbine Testing and Evaluation, Part 1: "Power Performance Testing"
IEA recommendation edited by
S. Frandsen, A. Trenka and B.M. Pedersen

REF. 2. Parameterstudium af LM 12 m vinge. Måling af effektkurver og bremseevne for LM 12 m vinge monteret på Micon M 450 - 250 kW vindmølle.
Tripod Consult. Rapport TWD-880620-1. 1988 DK.

REF. 3. Fluid Dynamic Aspects of Wind Energy Conversion
AGARDOGRAPH 243.
O. De Vries. 1979

REF. 4. The Actuator Cylinder. A Flow Model for Vertical Axis Wind Turbines.
H.A. Madsen. IICET Aalborg University Centre 1982 Denmark.

REF. 5. Aerodynamisk og svingningsteoretisk undersøgelse af en Darrieusrotor. Risø M-2451 Bd 1 og 2.
U.S.Paulsen, J. Sørensen, J.E. Nielsen Risø 1985

REF. 6. Optimization of the Performance of the Variable Pitch Vertical Axis Wind Turbine.
A. Zervos, S.Dessipris, N. Athanassiadis. Proceeding of European Wind Energy Conference 1984, Hamburg FRG. pp 411-416.

REF. 7. A 2-D Flow Mortal for the Horizontal Axis Wind Turbine.
J. Van Briel, J. Van Leuwen, Proceedings of the 1984 Sixth BWEA Wind Energy Conference pp 301-312.

REF. 8. A Vortex-Wake Analysis of a Horizontal Axis Wind Turbine and a Comparison with a Modified Blade-Element Theory.
M.B. Anderson H1 Proceedings from 3'd International Wind Energy Systems, Copenhagen DK pp. 357-774.

REF. 9. Wind turbine Flow Field Model.
R.E. Wilson. Journal of Solar Energy Engineering 1986 No 4 pp 344-345

REF.10. Application of Actuator Surface Theory on Wind Turbines.
H.A. Madsen. Met. and Wind Energy Department, Annual Progress Report RR-544 1.January-31. December 1986. pp. 65-83.

REF.11. Aerodynamics of Propulsion.
D. Küchemann, J.Weber, Mc Craw-Hill Brook Comp. 1953 1.edition

REF.12. Hot-wire Measurements in the Wake of a Darrieus Rotor
A. Michos, G. Bergeles, N. Athanassiadis. Proceedings of European Wind Energy Conference 1984 in Hamburg FRG. pp 517-522.

REF.13. Hot-wire Measurements of the Flow Field in the Vicinity of a HAWT Rotor.
A. Papaconstantantinou, G. Bergeles. Journal of Wind Engineering and Industrial Aerodynamics 31 (1988) pp. 133-146.

REF.14. Windmill Flow Field with non-uniform Approach Flow.
M.A. Kotb and J. A. Schetz. Proceedings of European Wind Energy Conference 1984 in Hamburg, FRG. pp. 500-505.

REF.15. Nibe Wake 2 Datareport, Power Spectra.
J. Højstrup. (1988) Internal Report

REF.16. Wind Energy from turbulence: Constant Tip Speed Ratio Operation.
J.F. Manwell, R. H. Kirchhoff. Solar Energy Vol 34 No 1. pp. 59-67, 1985.

REF.17. Wind Energy Converters in a Real Windfield: Calculation of Hourly Mean Power Output.
H.G. Beyer, G.J. Gerdes, Wind Engineering Vol(10) No 21986.

REF.18. Simplified Rotor Loads from Wind Turbulence.
P.H. Madsen. Collection of several papers presented at EWEC 86 Herning Denmark. pp.81-86

REF.19. On Uncertainties in Power Performance Measurements.
S. Frandsen. Presented at 6'ASME Conference in Dallas Texas 1987 pp. 157-170.

REF.20. The Lammefjord Experiment.
M.S. Courtney. Presented at Windpower 1987 San Fransisco pp. 124-129.

REF.21. Evaluation of Power Performance Testing Proceedings by means of Measurements on a 90 kW Wind Turbine.
T. F. Pedersen, S.M. Petersen. Presented at Herning DK, Conference 1988 pp. 453-459.

REF.22. Accuracy of Power Curve Measurements. Edited by C.J. Christensen, J.B. Dragt . Risø-M-2632

REF.23. Errors in Wind Turbine Energy Production Estimates W.A. Vachon. Presented at 4'ASME Wind Energy Symposium, USA 1985 pp 227-230.

REF.24. Three-Dimensional Wind Simulation. P.S. Veers. Paper presented at 8'ASME Wind Energy Symposium pp 23-31.

REF.25. Estimation of Turbulence Variance and Scale, Simplified for Wind Turbine Applications. D.C. Powell. Paper presented at 8'ASME Wind Energy Symposium pp. 9-22.

Risø National Laboratory **Risø – M – 2835**

THE IMPACT OF THE INDUCED VELOCITY IN THE NEAR FLOW FIELD OF A HORIZONTAL AXIS WIND TURBINE

Uwe Schmidt Paulsen
The Test Station for Wind Turbines
Department of Meteorology and Wind Energy

Date December 1989

Department or group
The Test for Wind Turbines

Groups own registration number(s)

Project/contract no.

Pages 91 Tables 15 Illustrations 37 References 32

ISBN 87-550-1595-6

Abstract (Max. 2000 char.)
The report describes extensive power performance investigation on a Vestas V20 100 kW Prototype wind turbine. The measurements carried out and reported here comprises the experimental and theoretical results on power performance and induced wind speed effects derived at different cup anemometer locations. The report reviews in a separate annex recent development of measurements and theoretical models of the flow.

Descriptors – EDB

ACCURACY; ANEMOMETERS; ERRORS; FLOW MODELS; HORIZONTAL AXIS TURBINES; IDEAL FLOW; MEASURING METHODS; PERFORMANCE; PERFORMANCE TESTING; REVIEWS; SITE CHARACTERIZATION; STAGNATION; TURBULENT FLOW; VELOCITY; WIND

Available on request from Risø Library, Risø National Laboratory, (Risø Bibliotek, Forskningscenter Risø), P.O. Box 49, DK-4000 Roskilde, Denmark.
Telephone 42 37 12 12, ext. 2268/2269. Telex: 43116, Telefax: 46 75 56 27

Available on exchange from:
Risø Library,
Risø National Laboratory, P.O. Box 49,
DK-4000 Roskilde, Denmark
Phone +45 42 37 12 12, ext. 2268/2269
Telex 43 116, Telefax +45 46 75 56 27

ISBN 87-550-1595-6
ISSN 0418-6435